行政院國家科學委員會專題研究計畫 成果報告

奈米圖樣化的二維電子系統中拓樸絕緣體物理之研究
研究成果報告(精簡版)

計 畫 類 別 ：個別型
計 畫 編 號 ：NSC 100-2112-M-009-019-
執 行 期 間 ：100 年 08 月 01 日至 101 年 07 月 31 日
執 行 單 位 ：國立交通大學電子物理學系（所）

計 畫 主 持 人：朱仲夏

計畫參與人員：碩士班研究生-兼任助理人員：劉悌鐳
碩士班研究生-兼任助理人員：陳文長
碩士班研究生-兼任助理人員：林儀珓
博士班研究生-兼任助理人員：邱志宣
博士班研究生-兼任助理人員：張榮興
博士後研究：王律堯

報 告 附 件 ：出席國際會議研究心得報告及發表論文

公 開 資 訊 ：本計畫可公開查詢

中 華 民 國 101 年 11 月 05 日

中 文 摘 要 ： 我們用理論探索在奈米圖模下二維電子氣可能實現的人造拓樸絕緣體。二維電子氣的
高遷移率與成熟的製程技術吸引對於拓樸絕緣體上較完計畫
標題:研究在奈米圖模下
二維電子氣的拓樸絕緣體物理
1. 去探索奈米圖模下二維電子氣具有的拓樸絕緣體物理
2. 對以後的研究建立一個在二維電子氣的製程科技可實現的新穎機能基礎理論框架
整尺度物理研究的可能性。我們特別關注的是自旋軌道交互作用,包含本質自旋軌道交
互作用,像在奈米圖模下二維電子氣的 Rahsba, Dresselhaus 自旋軌道交互作用。這些
效應造成的能隙打開和邊緣態將被研究。
奈米圖模下二維電子氣包括中空圓,奈米閘極和磁通量晶格之各種形式晶格將被研
究。自旋軌道交互作用可由均勻或週期的閘極圖模所造成。探討拓樸絕緣體對晶格具
有和不具有反轉對稱的相關性質。中空圓使用硬牆式位能而鬆餅形位能可使用奈米閘
極控制。研究在高對稱點 K,M,Γ 上由於自旋軌道交互作用引起的能階交叉和能隙打開,
以及其他在布里淵區內的 k 點。布洛赫函數可用晶格中心的圓柱形波函數構成,將之推
廣到二維磁通量晶格由於自旋軌道交互作用引起的能隙打開,對於每個佔據能帶可以
計算 Berry 曲率和 Chern 數。透過直接計算邊緣態的波函數以及色散關係可以引入適
當的邊界條件。我們特別想探討樣品邊緣方向性對於邊緣態的相關性。
我們的目標是對以後研究建立一個在二維電子氣可實現的新穎機能理論框架。

中文關鍵詞： 拓樸絕緣體,奈米圖模,奈米閘極,邊緣態,自旋軌道交互作用,磁通量晶格,鬆餅形位

英 文 摘 要 ： Title of the proposal: A study on the topological insulator physics in nano-patterned 2DEG
The goals in this study are
1. to explore the topological insulator physics in nano-patterned 2DEG,
2. to establish a basic theoretical framework for later study on novel functionalities

made possible by the 2DEG fabrication technologies. We propose to explore theoretically the possibility of realizing artificial topological insulator (TI) in nano-patterned two-dimensional electron-gas (2DEG). The high mobility of the 2DEG and the associated sophisticated fabrication technologies already established for 2DEG make this possibility attractive for a fuller scale study on the TI physics.

Particular attention will go to the effects of spin-orbit interactions (SOI), including intrinsic SOIs such as the Rashba-type and Dresselhaus-type SOIs, on the nano-patterned 2DEG. Their effects on gap opening and edge states will be studied.

Nano-patterned 2DEG includes void lattices, nano-gate lattices and magnetic flux lattices. The SOIs considered are either uniform or periodic, in direct correspondence to the gate pattern. Lattices with inversion and without inversion symmetry will be studied to explore its connection to the robustness of the TI effects. Various types of lattices will be studied.

Hard wall potential model will be used for the void and muffin-tin potential model will be used for the nano-gate. Features of energy level crossing or gap opening will be studied at the high symmetry points, such as the K, M, and the Γ points, and at other k points in the Brillouin zone. Detail analysis of the Bloch wavefunction in terms of the cylindrical wavefunctions centered at a lattice site will be carried out and the insights will be applied to the study of magnetic flux lattices in 2DEG. Gap opening due to SOI, the effects on the corresponding Berry curvature and the Chern number for each such occupied band will be calculated. Appropriate boundary conditions will be introduced for a direct calculation of the edge state dispersions and edge state wavefunction. In

particular, the dependence of the edge states on the orientation of the edges will be explored.
In all, we aim at establishing a theoretical framework for later study on novel functionalities made possible by the 2DEG.

英文關鍵詞： topological insulators, nano-patterned, nano-gate, edge state, spin-orbit

行政院國家科學委員會補助專題研究計畫 ■成果報告 □期中進度報告

（計畫名稱）奈米圖樣化的二維電子系統中拓樸絕緣體物理之研究

計畫類別：■個別型計畫　□整合型計畫
計畫編號：NSC　100 － 2112 － M － 009 － 019 －
執行期間： 2011 年 8 月 1 日至 2012 年 7 月 31 日

執行機構及系所：

計畫主持人：　朱仲夏
共同主持人：
計畫參與人員：博士後: 王律堯
博士生: 張榮興，邱志宣
碩士生: 陳文長，劉悌鐳，林儀玹

成果報告類型(依經費核定清單規定繳交)：■精簡報告　□完整報告

本計畫除繳交成果報告外，另須繳交以下出國心得報告：
□赴國外出差或研習心得報告
□赴大陸地區出差或研習心得報告
■出席國際學術會議心得報告
□國際合作研究計畫國外研究報告

處理方式：除列管計畫及下列情形者外，得立即公開查詢
□涉及專利或其他智慧財產權，□一年□二年後可公開查詢

中　華　民　國 101 年 10 月 31 日

中英文摘要及關鍵詞:

中文摘要:

我們用理論探索在奈米圖模下二維電子氣可能實現的人造拓樸絕緣體。二維電子氣的高遷移率與成熟的製程技術吸引對於拓樸絕緣體上較完計畫標題:研究在奈米圖模下二維電子氣的拓樸絕緣體物理

1. 去探索奈米圖模下二維電子氣具有的拓樸絕緣體物理
2. 對以後的研究建立一個在二維電子氣的製程科技可實現的新穎機能基礎理論框架

整尺度物理研究的可能性。我們特別關注的是自旋軌道交互作用,包含本質自旋軌道交互作用,像在奈米圖模下二維電子氣的 Rahsba, Dresselhaus 自旋軌道交互作用。這些效應造成的能隙打開和邊緣態將被研究。

奈米圖模下二維電子氣包括中空圓,奈米閘極和磁通量晶格之各種形式晶格將被研究。自旋軌道交互作用可由均勻或週期的閘極圖模所造成。探討拓樸絕緣體對晶格具有和不具有反轉對稱的相關性質。中空圓使用硬牆式位能而鬆餅形位能可使用奈米閘極控制。研究在高對稱點 K,M,Γ上由於自旋軌道交互作用引起的能階交叉和能隙打開,以及其他在布里淵區內的 k 點。布洛赫函數可用晶格中心的圓柱形波函數構成,將之推廣到二維磁通量晶格由於自旋軌道交互作用引起的能隙打開,對於每個佔據能帶可以計算 Berry 曲率和 Chern 數。透過直接計算邊緣態的波函數以及色散關係可以引入適當的邊界條件。我們特別想探討樣品邊緣方向性對於邊緣態的相關性。

我們的目標是對以後研究建立一個在二維電子氣可實現的新穎機能理論框架。

關鍵詞:拓樸絕緣體,奈米圖模,奈米閘極,邊緣態,自旋軌道交互作用,磁通量晶格,鬆餅形位能,能階交叉,能隙打開,Berry 曲率,Chern 數。

英文摘要:

Title of the proposal: A study on the topological insulator physics in nano-patterned 2DEG

The goals in this study are

1. to explore the topological insulator physics in nano-patterned 2DEG,
2. to establish a basic theoretical framework for later study on novel functionalities made possible by the 2DEG fabrication technologies.

We propose to explore theoretically the possibility of realizing artificial topological insulator (TI) in nano-patterned two-dimensional electron-gas (2DEG). The high mobility of the 2DEG and the associated sophisticated fabrication technologies already established for 2DEG make this possibility attractive for a fuller scale study on the TI physics. Particular attention will go to the effects of spin-orbit interactions (SOI), including intrinsic SOIs such as the Rashba-type and Dresselhaus-type SOIs, on the nano-patterned 2DEG. Their effects on gap opening and edge states will be studied.

Nano-patterned 2DEG includes void lattices, nano-gate lattices and magnetic flux lattices. The SOIs considered are either uniform or periodic, in direct correspondence to the gate pattern. Lattices with inversion and without inversion symmetry will be studied to explore its connection to the robustness of the TI effects. Various types of lattices will be studied.

Hard wall potential model will be used for the void and muffin-tin potential model will be used for the nano-gate. Features of energy level crossing or gap opening will be studied at the high symmetry points, such as the K, M, and the Γ points, and at other k points in the Brillouin zone. Detail analysis of the Bloch wavefunction in terms of the cylindrical wavefunctions centered at a lattice site will be carried out and the insights will be applied to the study of magnetic flux lattices in 2DEG. Gap opening due to SOI, the effects on the corresponding Berry curvature and the Chern number for each such occupied band will be calculated. Appropriate boundary conditions will be introduced for a direct calculation of the edge state dispersions and edge state wavefunction. In particular, the dependence of the edge states on the orientation of the edges will be explored.

In all, we aim at establishing a theoretical framework for later study on novel functionalities made possible by the 2DEG.

Keywords: topological insulators, nano-patterned, nano-gate, edge state, spin-orbit interaction, magnetic flux lattice, muffin-tin potential, energy level crossing, gap opening, Berry curvature,
Chern number.

報告內容:
Published works:

"Effects of edge potential on an armchair-graphene open boundary and nanoribbons"
Physical Review B 85, 155444 (2012)
C.H. Chiu and C.S. Chu

"Nonuniversality of the intrinsic inverse spin-Hall effect in diffusive systems"
Physical Review B 85, 165201 (2012)
L.Y. Wang, A.G. Mal'shukov, and C.S. Chu

"Robust level coincidences in the subband structure of quasi-2D systems"
Solid State Communications (2012) (accepted)
R. Winkler, L.Y. Wang, Y.H. Lin, and C.S. Chu

Works in preparation:

"Effects of spin-orbit interaction on the topological physics in a 2D triangular muffin-potential lattice"
R.S. Chang, W.L. Su, and C.S. Chu

Details of these above works are presented in the following.

Effects of edge potential on an armchair-graphene open boundary and nanoribbons

Chi-Hsuan Chiu and Chon-Saar Chu

Department of Electrophysics, National Chiao Tung University, Hsinchu 30010, Taiwan, Republic of China

(Received 17 December 2011; revised manuscript received 21 March 2012; published 23 April 2012)

Pseudospin flipping is found to be the key process leading to the formation of an edge-potential-induced edge state at an armchair-graphene open boundary and nanoribbons. At an open boundary, the edge potential U_0 is shown to turn on pseudospin-flipped (intravalley) scattering even though U_0 does not post an apparent breaking of the AB site (basis atoms) symmetry. For a valley-polarized incident beam, the interference between the pseudospin-conserving (intervalley) and -nonconserving (intravalley) processes in the scattering state leads to a finite out-of-plane pseudospin density. This two-wave feature in the evanescent regime leads to the formation of the edge state. The physical origin of the edge state is different from that for the Tamm states in semiconductors. For an armchair-graphene nanoribbon with a gapless energy spectrum, applying U_0 to both edges opens up an energy gap. Both edge states and energy gap opening exhibit distinct features in nanoribbon conductance.

DOI: 10.1103/PhysRevB.85.155444 PACS number(s): 73.22.Pr, 72.80.Vp, 73.20.−r

I. INTRODUCTION

Ever since the experimental separation of its sample,[1,2] graphene has become a fascinating paradigm for the germination of novel physical phenomena[3–8] and future applications in carbon-based nanoelectronics.[9–14] This is due to the fact that the low-energy physics in graphene is that of a two-dimensional massless Dirac particle,[1,15] and also to its striking material properties of high electronic mobility[16] and thermal conductivity.[17] The structure of graphene, a single honeycomb lattice layer of carbon atoms, has provided two additional twists, or degrees of freedom, to the Dirac physics. Pseudospin,[18–20] or the sublattice pseudospin, arises from the bipartite honeycomb lattice, which consists of two distinct triangular sublattices. Valley isospin[21–23] arises from two nonequivalent K and K' points (Dirac points) at the corners of the Brillouin zone. These have contributed to anomalous physical characteristics in phenomena such as Klein tunneling,[15,24,25] quantum Hall effects,[26,27] weak (anti)localization,[28–30] focusing of electron flow in a graphene p-n junction,[31] and electron beam supercollimation.[18]

Edge states at a zigzag edge of graphene nanostructures has attracted an immense amount of attention recently.[32–50] These one-dimensional (1D) extended states, localized near the system edge, are zero-energy states of topological origin, and are the result of particle-hole symmetry.[35] The flatband nature of the edge states contributes to the large density of states in neutral zigzag graphene nanoribbons (GNRs) at the Fermi energy, and leads to localized magnetic structures at the zigzag edges.[33] Recent scanning tunneling spectroscopy measurements on chiral GNRs,[48] with a regular mixing of zigzag and armchair edges, reveals the presence of 1D GNR edge states.[48,49] There have been promising efforts to fabricate ideal GNRs with only zigzag or armchair edges.[51,52] The energy spectrum of the zigzag GNR is gapless because of the edge states.[5,33] On the other hand, the flatband feature of the edge states could support an energy gap when a Hubbard term for the on-site Coulomb repulsion is included.[33,46,48]

Edge potentials were invoked recently for the study of gap opening and gap modulation in the zigzag GNR.[45,47] For edge potentials applying along the GNR edges taking up either a δ profile[45] or a finite range profile across the GNR width,[47] the GNR energy spectrum opens up a gap when the applied potential is antisymmetric over the width of the GNR.[45,47] Meanwhile, the edge potential is also invoked to convert the flatband edge states into valley-dependent gapless edge states.[43] An on-site energy U_0 at the boundary is shown, when the U_0 magnitude is large enough, to suppress the hopping onto the outermost sites and to change the edge to that of a bearded edge.[43] In the presence of a bulk energy gap Δ, due to a staggered sublattice potential, the continuous U_0 tuning of the edge-state dispersion relation between the zigzag-edge type and the bearded-edge type causes, at intermediate U_0 values, the conversion of the flatband edge states into gapless edge states that span the bulk energy gap.[43] The topological nature of these edge states derives from the fact that the states involve essentially only one valley (K or K'), and that the topological charge[53] $\tilde{N}_3 = \frac{1}{2}\tau_z \mathrm{sgn}(\Delta)$ is nonzero for a valley.[43] Here $\tau_z = \pm$ is the valley index.

The armchair edge of graphene, on the other hand, has no edge states.[33–35,54] It is of interest then to consider the use of the edge potential for possible generation and tuning of the edge states. In this paper, we show that the edge potential U_0 at an open boundary does cause the formation of edge states, and the key is its turning on of the pseudospin-flipped (intravalley) scattering process. With this scattering process enabled, an incident wave in one valley will be reflected, at an armchair open boundary, into two scattered waves associated, separately, with K and K' valleys. The interference between the two scattered waves gives rise to out-of-plane pseudospin density, which is of interest in its own right. As for the edge-state formation, the two-wave feature is important because it opens up both evanescent waves, from K and K' valleys, for the construction of the edge-state wave function. Even though the two evanescent waves have different pseudospins, we show that the edge potential can provide the needed pseudospin rotation at the boundary for the edge-state boundary condition. Two interesting edge-state features are worth noticing here. The states are dispersive, and their formation does not require a finite threshold in U_0. The fact that the edge states are generated for arbitrary nonzero U_0 shows unequivocally that the physical origin is not Tamm-type[55]—the type of edge states induced, or trapped, by a sufficiently strong trapping potential at the

system boundary. Rather, the role of U_0 is to summon both evanescent waves for the formation of the edge states.

The effects of the edge potential on armchair GNRs are also explored in this work, with edge potentials that are symmetrically configured. Gap opening in the energy spectrum is obtained in addition to the aforementioned edge-state generation. To best illustrate the gap-opening features, we consider armchair GNRs that are gapless in their unperturbed energy spectrum by judiciously choosing the GNR widths.[33,38,39,56] Our finding shows that the energy gap (a global gap) is formed, at $\mathbf{k} = \mathbf{0}$, when an edgelike branch splits out of and in between GNR subbands. States in the edgelike branch have an edgelike spatial profile, except in the long wave-vector regime ($\mathbf{k} \approx \mathbf{0}$), where the spatial profile becomes bulklike. Interestingly, we can find an energy interval within which the edge states exist while the bulklike states do not. The characteristics in the GNR conductance associated with this energy interval are identified. As the propagation direction of the edge states is correlated with the pseudospin, it is expected that the edge states are insensitive to disorder. The scattering wave formulation which we have implemented in this work facilitates extraction of analytical results for better physical understanding. All our results compare well with direct numerical calculations.

This paper is organized as follows. In Sec. II, we present our scattering wave approach to an armchair-graphene open boundary in the presence of an edge potential U_0. The boundary condition is cast in a pseudospin scattering form most convenient for our discussion. For the scattering states, the out-of-plane pseudospin density is presented. For the edge states, an explicit form for the pseudospin rotation operator due to U_0 at the open boundary is presented. The edge-state dispersion relation is obtained numerically while its long-wavelength expression is obtained analytically. In Sec. III, we present our results for the armchair GNR due to a symmetrically configured edge potential. The finite-size effect on the edgelike branch and the gap opening in the GNR energy spectrum are presented. The effects of the edge potential on the armchair GNR conductance are also presented in Sec. IV. Finally, a conclusion is presented in Sec. V.

II. ARMCHAIR GRAPHENE OPEN BOUNDARY

In this section, we present a scattering approach for the study of edge-potential effects on a armchair graphene open boundary. This approach allows us to extract, analytically, physical pictures such as the edge-potential-induced pseudospin scattering, the out-of-plane pseudospin density, and the edge-potential-induced edge states. In particular, the analytic expression for the edge-state dispersion relation in the long-wavelength regime shows that the edge states are generated for an arbitrary finite edge potential. This indicates that the edge state is not of Tamm-type. All the features found in this section will form the basis for the understanding of the edge-potential effects on the GNR in the next section.

A. Basic model and a scattering approach

The conventions and notations that we adopt in this work are described briefly below in the introduction of our basic model. The tight-binding Hamiltonian[5] for a armchair graphene open

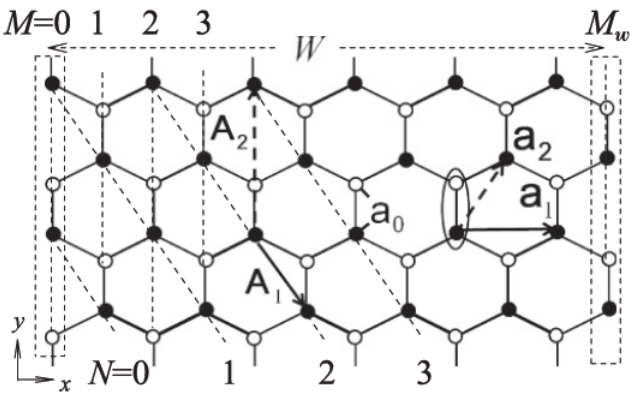

FIG. 1. Armchair GNR with unit-cell coordinates M (vertical dotted lines) and N (slanted dotted lines). Edges of the GNR are at $M = 0$ and M_w. Indicated are sites A (•) and B (○); Bravais lattice vectors $\mathbf{A}_1 = \mathbf{a}_1 - \mathbf{a}_2$ and $\mathbf{A}_2 = -\mathbf{a}_1 + 2\mathbf{a}_2$, where $\mathbf{a}_1 = 2a\hat{x}$ and $\mathbf{a}_2 = a\hat{x} + \sqrt{3}a\hat{y}$, and $a = \sqrt{3}a_0/2$, with C–C bond length $a_0 = 1.42$ Å.

boundary is given by

$$H = H_{\text{bulk}} + H_{\text{edge gate}}, \tag{1}$$

where

$$\begin{aligned} H_{\text{bulk}} &= -\gamma_0 \sum_{\langle i,j \rangle} \left(\hat{A}^\dagger_{\mathbf{R}_i} \hat{B}_{\mathbf{R}_j} + \hat{B}^\dagger_{\mathbf{R}_j} \hat{A}_{\mathbf{R}_i} \right), \\ H_{\text{edge gate}} &= \sum_i U_0 \left(\hat{A}^\dagger_{\mathbf{R}_i} \hat{A}_{\mathbf{R}_i} + \hat{B}^\dagger_{\mathbf{R}_i} \hat{B}_{\mathbf{R}_i} \right). \end{aligned} \tag{2}$$

The operators $\hat{A}^\dagger_{\mathbf{R}_i}$ and $\hat{A}_{\mathbf{R}_i}$ create and annihilate electrons at the A site of the ith unit cell, respectively, with cell coordinates (M_i, N_i) and cell location $\mathbf{R}_i = M_i\mathbf{A}_1 + N_i\mathbf{A}_2$, where $\mathbf{A}_1$ and $\mathbf{A}_2$ are Bravais lattice vectors. In terms of the more familiar Bravais lattice vectors $\mathbf{a}_1 = 2a\hat{x}$ and $\mathbf{a}_2 = a\hat{x} + \sqrt{3}a\hat{y}$ (see Fig. 1), we have $\mathbf{A}_1 = \mathbf{a}_1 - \mathbf{a}_2$ and $\mathbf{A}_2 = -\mathbf{a}_1 + 2\mathbf{a}_2$. Here $a = \sqrt{3}a_0/2$ and $a_0 = 1.42$ Å is the C–C bond length. We note that our choice of the cell coordinates (M_i, N_i) is convenient for the armchair open boundary. Included in $\langle i,j \rangle$ are nearest-neighbor hoppings, with $\gamma_0 = 2.66$ eV. H_{bulk} includes only $M_{i,j} \geqslant 0$ due to the $M = 0$ armchair boundary. The edge potential $H_{\text{edge gate}}$ applies an on-site energy U_0 to the $M_i = 0$ sites. In all the expressions that follow, whenever appropriate, units for energy, length, and wave vector are chosen to be γ_0, a, and $K_0 = 2\pi/(3a)$, respectively.

Scattering states at the armchair open boundary are constructed out of the Bloch states of graphene, albeit restricting the unit-cell summation in these Bloch states to $M \geqslant 0$. Specifically, Fig. 2 shows that the scattering state consists of an incident wave $|\Psi^{\text{B}}_{\mathbf{k}_\alpha}\rangle$, and intervalley and intravalley scattered waves $|\Psi^{\text{B}}_{\mathbf{k}_\beta}\rangle$ and $|\Psi^{\text{B}}_{\mathbf{k}_\gamma}\rangle$, respectively, given by

$$\left|\Psi^{(\text{sc})}_{\mathbf{k}_\alpha}\right\rangle = \left|\Psi^{\text{B}}_{\mathbf{k}_\alpha}\right\rangle + r_1 \left|\Psi^{\text{B}}_{\mathbf{k}_\beta}\right\rangle + r_2 \left|\Psi^{\text{B}}_{\mathbf{k}_\gamma}\right\rangle, \tag{3}$$

where r_1 (r_2) denotes the intervalley (intravalley) reflection coefficient. Here the Bloch states $|\Psi^{\text{B}}_{\mathbf{k}}\rangle$, given by

$$\left|\Psi^{\text{B}}_{\mathbf{k}}\right\rangle = \sum_{j,s} e^{i\mathbf{k}\cdot\mathbf{R}_j} C^{(s)}_{\mathbf{k}} \left|j,s\right\rangle, \tag{4}$$

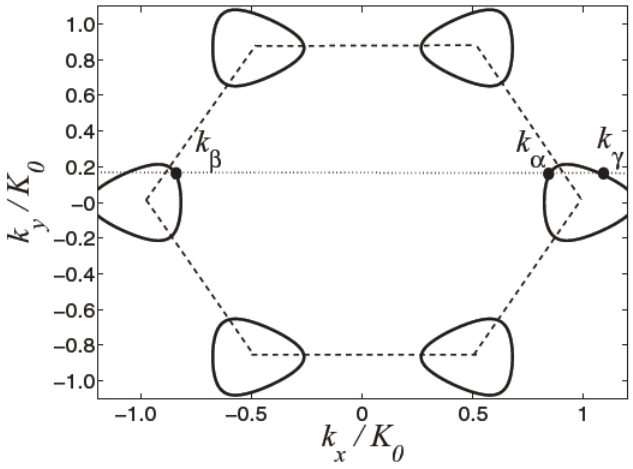

FIG. 2. States that involve reflection at the $M = 0$ open boundary in Fig. 1. Shown are the energy contour, the Brillouin zone boundary (dashed line), and valleys K (at $K_0\hat{x}$) and K' (at $-K_0\hat{x}$). The incident state is $\mathbf{k}_\alpha$ and the intervalley (intravalley) reflected state is $\mathbf{k}_\beta$ ($\mathbf{k}_\gamma$). The index for the left- (right-) going state is $\xi = 1(\bar{1})$. The index for the K (K') valley is $\eta = 1$ ($\bar{1}$). Here, $\alpha = (\xi,\eta) = (1,1)$, $\beta = (\bar{\xi},\bar{\eta})$, and $\gamma = (\bar{\xi},\eta)$.

sum over the unit-cell index j up to the open boundary ($M_j \geqslant 0$), and over the A (B) site index $s = 1$ (2). This scattering state approach has an advantage over the direct numerical approach in that the asymptotic ($M \gg 1$) boundary condition is already taken care of by the Bloch states, and the scattering problem is reduced to the finding of only two reflection coefficients.

To set the stage for the pseudospin scattering processes in the next subsection, we provide the explicit form of the pseudospinor in the following:

$$\left(C_{\mathbf{k}}^{(1)}, C_{\mathbf{k}}^{(2)}\right)^T = N_{\mathbf{k}}\left(1, \pm\sqrt{H_{\mathbf{k}}\tilde{H}_{\mathbf{k}}}/H_{\mathbf{k}}\right)^T. \tag{5}$$

Here $N_{\mathbf{k}}$ is the normalization constant for the pseudospinor, and $\pm$ is for the conduction (valence) band. Furthermore, $H_{\mathbf{k}} = -\gamma_0[1 + 2e^{-i\sqrt{3}k_y a}\cos(k_x a)]$, whereas $\tilde{H}_{\mathbf{k}} = -\gamma_0[1 + 2e^{i\sqrt{3}k_y a}\cos(k_x a)]$. For real wave vector $\mathbf{k}$, $\tilde{H}_{\mathbf{k}} = H_{\mathbf{k}}^*$, so that $C_{\mathbf{k}}^{(2)} = H_{\mathbf{k}}^*/(\sqrt{2}\,|H_{\mathbf{k}}|)$ carries the phase of $H_{\mathbf{k}}^*$, and the pseudospin orientation is in-plane.

In contrast, the pseudospin orientation becomes out-of-plane when $\mathbf{k}$ is complex. For our purposes here, k_x is determined from

$$\cos(k_x a) = -\frac{1}{2}\cos(\sqrt{3}k_y a) + \frac{\xi\eta}{2}\sqrt{E^2 - \sin^2(\sqrt{3}k_y a)} \tag{6}$$

for a given k_y and energy E. A complex k_x is conveniently cast in the form $k_x = \eta\kappa_r - i\xi\kappa_i$, where κ_r and κ_i are positive, and $\eta = 1$ ($\bar{1}$) denotes the K (K') valley, while $\xi = 1$ ($\bar{1}$) denotes the left- (right-) going state. We have $k_{\beta x} = -k_{\alpha x}$ for intervalley reflection and $k_{\gamma x} = k_{\alpha x}^*$ for intravalley reflection. Since both $H_{\mathbf{k}}$ and $\tilde{H}_{\mathbf{k}}$ are even in k_x, regardless of whether k_x is real or complex, the pseudospins for $k_{\alpha x}$ and $k_{\beta x}$ are the same, but they are different from the pseudospin for $k_{\gamma x}$.

It is known[5] that scattering at a pristine armchair graphene open boundary involves only intervalley reflection where pseudospin is conserved. Applying an edge potential $H_{\text{edge gate}}$ that affects equally the A and B site potentials in a unit cell seems not to have broken the equal preference of staying in either site, and thus it seems to be pseudospin-conserving. Our finding in the next subsection, however, shows the contrary.

B. Edge-potential-induced pseudospin scattering

In this subsection, we demonstrate the physical origin of pseudospin flipping due to the edge potential $H_{\text{edge gate}}$. Insight in this regard is obtained from the unit-cell recurrence relation. By substituting Eqs. (3) and (4) into Eq. (1) and focusing upon the coefficient of the term $e^{ik_y R_{jy}}$, the recurrence relations are obtained as

$$(-U_0 + \sigma_x)\,V_0 + \mathbf{T}V_1 = -EV_0, \tag{7a}$$

$$\mathbf{T}V_{M-1} + \sigma_x V_M + \mathbf{T}V_{M+1} = -EV_M, \tag{7b}$$

where $V_M = (\phi_M^{(1)}, \phi_M^{(2)})^T$ is the wave-function amplitude at the Mth unit cell, with

$$\phi_M^{(s)} = e^{ik_{\alpha x}Ma}C_{\mathbf{k}_\alpha}^{(s)} + r_1 e^{ik_{\beta x}Ma}C_{\mathbf{k}_\beta}^{(s)} + r_2 e^{ik_{\gamma x}Ma}C_{\mathbf{k}_\gamma}^{(s)}. \tag{8}$$

Equation (7b) is obtained from the coefficients at the Mth unit cell for $M > 0$ and energy E. Terms involving $\mathbf{T}$ and σ_x are from intercell and intracell hopping, respectively. Actually, the same equation gives the bulk recurrence relation for the Bloch states. On the other hand, Eq. (7a) carries the sole effect of the edge potential via the term $-U_0 V_0$. No unit cell of smaller M exists to contribute to the hopping, and the negative sign on U_0 follows from our sign convention for the hopping coefficient $-\gamma_0$. The hopping matrix $\mathbf{T}$ is given by

$$\mathbf{T} = \begin{pmatrix} 0 & e^{-i\sqrt{3}k_y a} \\ e^{i\sqrt{3}k_y a} & 0 \end{pmatrix}. \tag{9}$$

Equation (7) is cast into a compact form by borrowing a symbol V_{-1} from, mathematically, the bulk recurrence relation in Eq. (7b) to $M = 0$, and substituting it into Eq. (7a), to give

$$U_0 V_0 + \mathbf{T}V_{-1} = 0. \tag{10}$$

The expression for V_{-1} is given by Eq. (8), and Eq. (10) is expanded to give

$$\begin{pmatrix} U_0 C_{\mathbf{k}_\beta}^{(1)} + C_{\mathbf{k}_\beta}^{(2)} e^{-i\mathbf{k}_\beta\cdot\mathbf{a}_2} & U_0 C_{\mathbf{k}_\gamma}^{(1)} + C_{\mathbf{k}_\gamma}^{(2)} e^{-i\mathbf{k}_\gamma\cdot\mathbf{a}_2} \\ U_0 C_{\mathbf{k}_\beta}^{(2)} + C_{\mathbf{k}_\beta}^{(1)} e^{-i\mathbf{k}_\beta\cdot(\mathbf{a}_1-\mathbf{a}_2)} & U_0 C_{\mathbf{k}_\gamma}^{(2)} + C_{\mathbf{k}_\gamma}^{(1)} e^{-i\mathbf{k}_\gamma\cdot(\mathbf{a}_1-\mathbf{a}_2)} \end{pmatrix} \begin{pmatrix} r_1 \\ r_2 \end{pmatrix} = -\begin{pmatrix} U_0 C_{\mathbf{k}_\alpha}^{(1)} + C_{\mathbf{k}_\alpha}^{(2)} e^{-i\mathbf{k}_\alpha\cdot\mathbf{a}_2} \\ U_0 C_{\mathbf{k}_\alpha}^{(2)} + C_{\mathbf{k}_\alpha}^{(1)} e^{-i\mathbf{k}_\alpha\cdot(\mathbf{a}_1-\mathbf{a}_2)} \end{pmatrix}. \tag{11}$$

Rearranging into a form more convenient for our discussion on the reflection coefficients, we get

$$\begin{pmatrix} U_0 C_{\mathbf{k}_\beta}^{(1)} + C_{\mathbf{k}_\beta}^{(2)} e^{-i\mathbf{k}_\beta\cdot\mathbf{a}_2} \\ U_0 C_{\mathbf{k}_\beta}^{(2)} + C_{\mathbf{k}_\beta}^{(1)} e^{-i\mathbf{k}_\beta\cdot(\mathbf{a}_1-\mathbf{a}_2)} \end{pmatrix} r_1 + \begin{pmatrix} U_0 C_{\mathbf{k}_\gamma}^{(1)} + C_{\mathbf{k}_\gamma}^{(2)} e^{-i\mathbf{k}_\gamma\cdot\mathbf{a}_2} \\ U_0 C_{\mathbf{k}_\gamma}^{(2)} + C_{\mathbf{k}_\gamma}^{(1)} e^{-i\mathbf{k}_\gamma\cdot(\mathbf{a}_1-\mathbf{a}_2)} \end{pmatrix} r_2 = -\begin{pmatrix} U_0 C_{\mathbf{k}_\alpha}^{(1)} + C_{\mathbf{k}_\alpha}^{(2)} e^{-i\mathbf{k}_\alpha\cdot\mathbf{a}_2} \\ U_0 C_{\mathbf{k}_\alpha}^{(2)} + C_{\mathbf{k}_\alpha}^{(1)} e^{-i\mathbf{k}_\alpha\cdot(\mathbf{a}_1-\mathbf{a}_2)} \end{pmatrix}. \tag{12}$$

Equations (11) and (12) are two key relations in this work.

Taking $U_0 = 0$ in Eq. (12), we see that $r_1 = -e^{-2ik_{\alpha x}a}$ and $r_2 = 0$. This results from the fact that the $\mathbf{k}_\alpha$ and $\mathbf{k}_\beta$ states have the same pseudospin and the $\mathbf{k}_\gamma$ state has a different pseudospin. Furthermore, $(\mathbf{k}_\beta - \mathbf{k}_\alpha)\cdot\mathbf{a}_2 = (\mathbf{k}_\beta - \mathbf{k}_\alpha)\cdot(\mathbf{a}_1 - \mathbf{a}_2) = -2k_{\alpha x}a$. Pseudospin is conserved. Taking $U_0 \neq 0$, however, has effectively brought about other pseudospins. In fact, the on-site nature of U_0 has kept intact the pseudospins of the associated terms in Eq. (12), whereas the other terms have their $C_{\mathbf{k}}^{(s)}$ coefficients inverted due to their hopping origin. Thus r_2 can no longer remain zero, and pseudospin flipped reflection is invoked. It is clear that the turning on of the pseudospin flipped reflection does not require a threshold U_0, but rather a nonzero U_0.

A comment on our seemingly surprising result, namely that the edge potential $H_{\text{edge gate}}$ affects equally the A and B sites on the open boundary and can open up pseudospin flipped reflection, is in order here. Equation (12) clearly shows that pseudospins associated with U_0 have their in-plane nature kept intact. This is expected. What one might overlook, however, is that U_0 can still bring about pseudospins other than the incident one. Equation (12) shows that this is achieved by way of relative phases between the two components of a pseudospin.

C. Out-of-plane pseudospin density

As U_0 opens up a pseudospin flipped channel, interference between the pseudospins of the reflected waves will occur. Since the pseudospins are in-plane for real $\mathbf{k}$, the interference will lead to out-of-plane pseudospin.

In this subsection, we present the out-of-plane pseudospin polarization $\mathcal{PP}_{z\eta}$ in the vicinity of the $M = 0$ boundary. Incident states propagating along $+y$ with energy within ΔE and from one valley (index η) are included. The density $n_{s\eta}(E, M_j)$ in the jth unit cell is

$$n_{s\eta}(E, M_j) = \sum_{\mathbf{k}_\alpha}{}' \left|\langle j,s|\Psi_{\mathbf{k}_\alpha}^{(\text{sc})}\rangle\right|^2, \tag{13}$$

where the primed summation has restricted the energy to the range $E \leqslant E(\mathbf{k}_\alpha) \leqslant E + \Delta E$, and $k_{\alpha y} > 0$. Here s refers to the A (B) sites, and $\alpha = (1,\eta)$ for incident $\mathbf{k}_\alpha$. Equation (13), or $n_{s\eta}$, depends on M_j but not on N_j, as it should. The pseudospin polarization, as defined by

$$\mathcal{PP}_{z\eta} \equiv \frac{n_{A\eta} - n_{B\eta}}{n_{A\eta} + n_{B\eta}}, \tag{14}$$

is presented in Fig. 3, where M is used instead of M_j. The decay of $\mathcal{PP}_{z\eta}$ with M is due to the spread in the wave vector $\Delta k_x(E)$, the range of which is subjected to the restrictions imposed by the summation. This leads to a decrease in the decay length with increasing E, as is seen in Figs. 3(a)–3(d). Meanwhile, $\mathcal{PP}_{z\eta}$ changes sign as its valley-index η is changed, or as the incident wave vectors are changed, from $k_y > 0$ to $k_y < 0$. Finally, the magnitude of $\mathcal{PP}_{z\eta}$ increases with U_0, as is demonstrated in comparing Figs. 3(a) and 3(c).

This out-of-plane pseudospin distribution can be realized in the presence of a valley-polarized incident beam. The recent development in valleytronics and, in particular, proposals on valley-filter[21,23] and valley-polarized electron beams[22] are, thus, of direct relevance to this work.

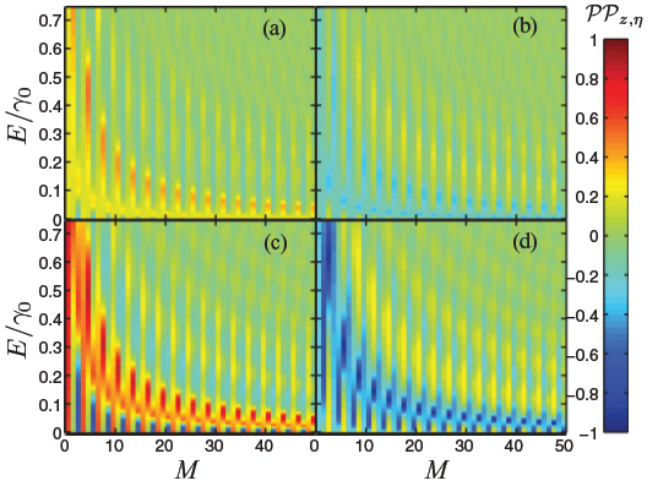

FIG. 3. (Color online) Contour plot of valley-dependent pseudospin polarization $\mathcal{PP}_{z\eta}$ against unit-cell location M and energy E. Edge potential $U_0 = 0.2$ in (a),(b) and $U_0 = 1.0$ in (c),(d). Contribution from K valley ($\eta = 1$) is shown in (a) and (c), and from K' valley ($\eta = -1$) is in (b) and (d). States within $\Delta E = 5 \times 10^{-3}$ are included. The sign of $\mathcal{PP}_{z\eta}$ reverses with η but the magnitude remains the same.

D. Edge-potential-induced edge states

In this subsection, we turn our attention to edge states, and we identify the key physical process that enables their formation. The pseudospin of these edge states, however, does not have an out-of-plane component. We will explain the reason for this in our analytical analysis.

Starting with Eq. (3), but without an incident component $|\Psi_{\mathbf{k}_\alpha}^{\text{B}}\rangle$, we look for edge-state energy E_{ed} for a given k_y in the complex k_x regime. Already, Eq. (11) has provided the basis for the numerical calculation of E_{ed}. This is from the zeros of the determinant of the matrix on the left-hand side of Eq. (11). The case for positive U_0's is illustrated in Fig. 4. Turning on U_0, an edge state branch is formed out of the bulk state continuum (gray area) on the valence-band side. Increasing U_0 pushes the branch away from the continuum. Near $U_0 = 1$, the edge-state branch has a zero slope near a Dirac cone. Beyond $U_0 = 1$, the slope in the long-wavelength regime increases monotonically with U_0 and approaches that of the continuum on the conduction-band side. A change in the sign of U_0 simply changes the sign of E_{ed}.

A number of interesting features about these edge states are in order here. These edge states are obtained without opening a gap in the bulk state continuum. The dispersion relations $E_{\text{ed}}(k_y)$ for all U_0 start and end at Dirac cones. These include cases when U_0 is arbitrarily small but nonzero. There is no threshold U_0, and this, in turn, assures us that the physics for this edge-state formation is not Tamm-type.[55] In fact, the edge-state formation is enabled by the opening up of the pseudospin flipped channel, and by a pseudospin rotation at the boundary. This pseudospin rotation analysis will be discussed in the last part of this subsection.

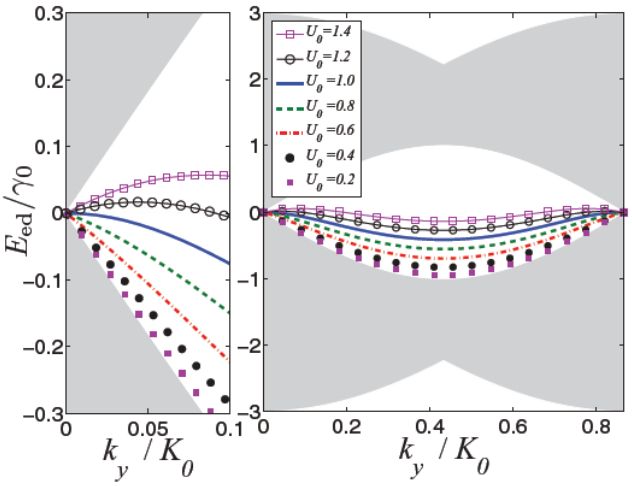

FIG. 4. (Color online) Edge-state dispersion relations induced by U_0 at an armchair open boundary are shown for $U_0 = 1.4$ (open square), 1.2 (open circle), 1 (solid curve), 0.8 (dashed curve), 0.6 (dashed-dotted curve), 0.4 (solid circle), and 0.2 (solid square). Gray areas depict the bulk electron continuum spectrum. Right panel shows a k_y range that includes two Dirac cones. Left panel shows a smaller k_y range.

An analytical expression for $E_{ed}(k_y)$ is derived near the Dirac cone, in the long-wavelength regime $k_y a_{2y} \ll 1$. This complements our numerical results given above for a better understanding. Assuming the form $E_{ed} = \alpha_1(U_0)|q_y|$, where $|q_y| = |k_y|a_{2y} \ll 1$, and the coefficient $\alpha_1(U_0)$, the U_0 it depends on is not necessarily small. We obtain, from Eq. (6), $k_x^\eta = (\eta K + \Delta k_{xr}^\eta) + i\Delta k_{xi}$. Here $\eta = 1$ and -1 correspond to cases for $\mathbf{k}_\gamma$ and $\mathbf{k}_\beta$, respectively. To lowest order in q_y, we have

$$\Delta k_{xi} = \frac{1}{\sqrt{3}}\sqrt{1-\alpha_1^2}|q_y| \equiv G(U_0)|q_y|,$$
$$\Delta k_{xr}^\eta = -\frac{\eta}{2\sqrt{3}}[1+G^2(U_0)]q_y^2, \tag{15}$$

where $G(U_0) = \frac{1}{\sqrt{3}}\sqrt{1-\alpha_1^2(U_0)}$. The coefficient $\alpha_1(U_0)$ is derived from requiring the determinant of the matrix in Eq. (11) to be zero. Using the relation $C_{\mathbf{k}}^{(2)}/C_{\mathbf{k}}^{(1)} = E_{ed}/H_{\mathbf{k}}$, we obtain, up to the second order in q_y,

$$\frac{-U_0\alpha_1}{1-U_0^2} = \sqrt{\frac{1-\alpha_1^2}{3}}. \tag{16}$$

Subsequently, in the $k_y a_{2y} \ll 1$ regime, we obtain

$$E_{ed} \approx \mathrm{sgn}(U_0)\frac{\sqrt{3}\left(U_0^2-1\right)}{\sqrt{1+U_0^2+U_0^4}}|k_y|a. \tag{17}$$

This is another key expression, which is valid to all orders in U_0.

The boundary condition, given by Eq. (12), must be in a pseudospin rotation form at the energy $E_{ed}(k_y)$, which connects pseudospins of the $\mathbf{k}_\beta$ and $\mathbf{k}_\gamma$ states. From Eq. (12), and dropping terms associated with $\mathbf{k}_\alpha$, we have

$$D_\beta \begin{pmatrix} C_{\mathbf{k}_\beta}^{(1)} \\ C_{\mathbf{k}_\beta}^{(2)} \end{pmatrix} r_1 + D_\gamma \begin{pmatrix} C_{\mathbf{k}_\gamma}^{(1)} \\ C_{\mathbf{k}_\gamma}^{(2)} \end{pmatrix} r_2 = 0, \tag{18}$$

where $D_\beta = [U_0 + e^{-ik_{\beta x}a}\mathbf{T}]$ and $D_\gamma = [U_0 + e^{-ik_{\gamma x}a}\mathbf{T}]$. This amounts to requiring $\mathscr{D} \equiv -(r_2/r_1)D_\beta{}^{-1}D_\gamma$ to rotate $\mathbf{k}_\gamma$'s pseudospin to that of the $\mathbf{k}_\beta$ state. The explicit form of $\mathscr{D}$ is

$$\mathscr{D} = -\frac{r_2/r_1}{\Lambda}\begin{pmatrix} 1-U_0^2e^{-2k_{xi}a} & ie^{-i\sqrt{3}k_y a}[2U_0e^{-k_{xi}a}\sin(k_{xr}a)] \\ ie^{i\sqrt{3}k_y a}[2U_0e^{-k_{xi}a}\sin(k_{xr}a)] & 1-U_0^2e^{-2k_{xi}a} \end{pmatrix}, \tag{19}$$

where $k_{xr} = \mathrm{Re}\,k_{\gamma x}$, $k_{xi} = \mathrm{Im}\,k_{\gamma x}$, and $\Lambda = U_0^2e^{-2k_{xi}a} - e^{i2k_{xr}a}$. The unimodular property of $\mathscr{D}$ has $\mathscr{D}(1,1) = \mathscr{D}^*(2,2)$, or $r_2/r_1\Lambda$ a real number, and the property $|\mathscr{D}(1,1)|^2 + |\mathscr{D}(1,2)|^2 = 1$ leads to $|r_2/r_1| = 1$, which is checked with our numerical results. We have thus demonstrated that the formation of the edge state requires the pseudospin rotation to satisfy a particular condition at the boundary, namely $|r_2/r_1| = 1$.

On the other hand, $\mathscr{D}$ can be expressed in terms of the orientation angles of the two pseudospins. The pseudospin states of $\mathbf{k}_\beta$ and $\mathbf{k}_\gamma$ are of the form $[\cos(\theta/2), \sin(\theta/2)e^{i\phi}]^T$ and $[\sin(\theta/2), \cos(\theta/2)e^{i\phi}]^T$, where θ and ϕ are real numbers representing the pseudospins' angles of orientation. As an operator that rotates an angle $\pi - 2\theta$ about an axis along $[\cos(\phi)\hat{x} + \sin(\phi)\hat{y}] \times \hat{z}$, we must also have

$$\mathscr{D} = \begin{pmatrix} \sin\theta & e^{-i\phi}\cos\theta \\ -e^{i\phi}\cos\theta & \sin\theta \end{pmatrix}. \tag{20}$$

Comparing Eqs. (19) and (20), we have

$$\sin\theta = -\left(1-U_0^2e^{-2k_{xi}a}\right)/|\Lambda|, \tag{21a}$$
$$\cos\theta = -(2U_0e^{-k_{xi}a}\sin k_{xr}a)/|\Lambda|, \tag{21b}$$
$$e^{-i\phi} = ie^{-i\sqrt{3}k_y a}. \tag{21c}$$

The relation $|r_2/r_1| = 1$ that the edge states are required to obey has important bearings on their pseudospin. Expressed in terms of θ and ϕ, the edge-state wave function $\Psi_{ed}(M)$ at the Mth unit cell, in pseudospin form, is given by

$$\Psi_{ed}(M) = r_1\, e^{ik_{\beta x}Ma}\begin{pmatrix} \cos(\theta/2) \\ \sin(\theta/2)e^{i\phi} \end{pmatrix} + r_2\, e^{ik_{\gamma x}Ma}\begin{pmatrix} \sin(\theta/2) \\ \cos(\theta/2)e^{i\phi} \end{pmatrix},$$

from which we calculate the pseudospin polarization $\mathcal{PP}_{z,\mathrm{ed}}(M)$, and we obtain

$$\mathcal{PP}_{z,\mathrm{ed}}(M) \equiv \frac{\Psi_{\mathrm{ed}}^{\dagger}\sigma_z\Psi_{\mathrm{ed}}}{\Psi_{\mathrm{ed}}^{\dagger}\Psi_{\mathrm{ed}}} = 0. \tag{22}$$

The fact that $\mathcal{PP}_{z,\mathrm{ed}}$ is zero in Eq. (22) is clearly seen from $\Psi_{\mathrm{ed}}^{\dagger}\sigma_z\Psi_{\mathrm{ed}} = e^{-2\,\mathrm{Im}(k_{\beta x})Ma}\cos\theta\,(|r_1|^2 - |r_2|^2)$, which vanishes when $|r_2/r_1| = 1$.

III. ARMCHAIR-GRAPHENE NANORIBBON

In this section, the effects of the edge potential on armchair GNR are studied. The scattering approach we invoked in the previous section is applied here, and simplifications in both the formulation and subsequent analysis are achieved. Features studied include the generation of edge states, their hybridization due to finite ribbon widths, band-gap modulation, and pseudospin characteristics. An expression for the band gap, up to second order in U_0, is obtained. In addition, an energy window in the electron spectrum is found within which the states are all edge states.

A. Formulation with scattering approach

The armchair GNR (see Fig. 1) has edges at $M = 0$ and M_w, and a total number of sites $W = M_w + 1$ across the width. The edge potential $H_{\text{edge gate}}$ in Eq. (2) now has $M_i = 0$ and M_w. Following Eq. (3), the GNR eigenstates $|\Psi^{(\mathrm{NR})}\rangle$ consist of four Bloch states, all of the form given by Eq. (4) but with the sum over the unit-cell index j restricted to the interval $0 \leqslant M_j \leqslant M_w$. For convenience of presentation, we label Bloch states that correspond to the K valley as A and B, with their $(\xi,\eta) = (\bar{1},1)$ and $(1,1)$, respectively. Bloch states that correspond to the K' valley are labeled C and D, with their $(\xi,\eta) = (1,\bar{1})$ and $(\bar{1},\bar{1})$, respectively. For a given k_y and energy E, we have

$$|\Psi^{(\mathrm{NR})}\rangle = \mathcal{A}\left|\Psi^{\mathrm{B}}_{\mathbf{k}_\mathrm{A}}\right\rangle + \mathcal{B}\left|\Psi^{\mathrm{B}}_{\mathbf{k}_\mathrm{B}}\right\rangle + \mathcal{C}\left|\Psi^{\mathrm{B}}_{\mathbf{k}_\mathrm{C}}\right\rangle + \mathcal{D}\left|\Psi^{\mathrm{B}}_{\mathbf{k}_\mathrm{D}}\right\rangle. \tag{23}$$

These coefficients are connected by reflections at the boundaries, given by

$$\begin{pmatrix} -1 & r_{\mathrm{AB}} & r_{\mathrm{AC}} & 0 \\ \tilde{r}_{\mathrm{BA}} & -1 & 0 & \tilde{r}_{\mathrm{BD}} \\ \tilde{r}_{\mathrm{CA}} & 0 & -1 & \tilde{r}_{\mathrm{CD}} \\ 0 & r_{\mathrm{DB}} & r_{\mathrm{DC}} & -1 \end{pmatrix} \begin{pmatrix} \mathcal{A} \\ \mathcal{B} \\ \mathcal{C} \\ \mathcal{D} \end{pmatrix} = 0. \tag{24}$$

Here $r_{\nu\mu}$ denotes the reflection coefficient at the $M = 0$ edge from Bloch states μ to ν, and $\tilde{r}_{\nu\mu}$ denotes reflection at the $M = M_w$ edge.

In this work, the applied edge potential is symmetric with respect to the center of the ribbon. Thus Eq. (24) can be simplified further by exploiting the parity symmetry. This is carried out by replacing R_{jx} by $R_{jx} - M_w a/2$ in the unit-cell summation of $|\Psi^{\mathrm{B}}_{\mathbf{k}_\nu}\rangle$. The parity of the nanoribbon eigenstate $|\Psi^{(\mathrm{NR})}\rangle$ is imposed by the relations $\mathcal{C} = \pm\mathcal{A}$ and $\mathcal{B} = \pm\mathcal{D}$, where the upper (lower) sign corresponds to even (odd) parity. Equation (24) is reduced to

$$\begin{pmatrix} 1 \mp r_{\mathrm{AC}} & \mp r_{\mathrm{AB}} \\ \mp r_{\mathrm{DC}} & 1 \mp r_{\mathrm{DB}} \end{pmatrix} \begin{pmatrix} \mathcal{C} \\ \mathcal{B} \end{pmatrix} = 0. \tag{25}$$

The energy spectrum for each parity is determined separately, according to Eq. (25). Level anticrossing thus occurs only between states of the same parity because the edge potential preserves the symmetry. For our convenience below, the reflections from states {B,C} into states {A,D} are represented by the reflection of state $\alpha = (\xi = 1,\eta)$ into states $\beta = (\bar{\xi},\bar{\eta})$ and $\gamma = (\bar{\xi},\eta)$. The reflection coefficients in Eq. (25) are then labeled as $r_{1\alpha}$ and $r_{2\alpha}$, with subscript 1 (2) denoting intervalley (intravalley) reflection. These coefficients are obtained, following a similar procedure that leads to Eq. (11), as

$$\begin{pmatrix} e^{-ik_{\beta x}M_w a/2}\left[U_0\,C^{(1)}_{\mathbf{k}_\beta} + C^{(2)}_{\mathbf{k}_\beta}e^{-i\mathbf{k}_\beta\cdot\mathbf{a}_2}\right] & e^{-ik_{\gamma x}M_w a/2}\left[U_0\,C^{(1)}_{\mathbf{k}_\gamma} + C^{(2)}_{\mathbf{k}_\gamma}e^{-i\mathbf{k}_\gamma\cdot\mathbf{a}_2}\right] \\ e^{-ik_{\beta x}M_w a/2}\left[U_0\,C^{(2)}_{\mathbf{k}_\beta} + C^{(1)}_{\mathbf{k}_\beta}e^{-i\mathbf{k}_\beta\cdot(\mathbf{a}_1-\mathbf{a}_2)}\right] & e^{-ik_{\gamma x}M_w a/2}\left[U_0\,C^{(2)}_{\mathbf{k}_\gamma} + C^{(1)}_{\mathbf{k}_\gamma}e^{-i\mathbf{k}_\gamma\cdot(\mathbf{a}_1-\mathbf{a}_2)}\right] \end{pmatrix} \begin{pmatrix} r_{1\alpha} \\ r_{2\alpha} \end{pmatrix}$$
$$= \begin{pmatrix} e^{-ik_{\alpha x}M_w a/2}\left[U_0 C^{(1)}_{\mathbf{k}_\alpha} + C^{(2)}_{\mathbf{k}_\alpha}\,e^{-i\mathbf{k}_\alpha\cdot\mathbf{a}_2}\right] \\ e^{-ik_{\alpha x}M_w a/2}\left[U_0 C^{(2)}_{\mathbf{k}_\alpha} + C^{(1)}_{\mathbf{k}_\alpha}\,e^{-i\mathbf{k}_\alpha\cdot(\mathbf{a}_1-\mathbf{a}_2)}\right] \end{pmatrix}. \tag{26}$$

Numerical results from this scattering approach compare well with exact diagonalization results. Moreover, Eqs. (26) and (25) provide a useful starting point for the derivation of the edge-potential-induced gap modulation, to be presented in a later subsection.

B. GNR energy spectrum

In the following, we present the energy spectrum of armchair GNR under the effect of edge potentials. To better illustrate the edge-potential-induced gap-opening features, the GNRs considered here are of the type $W = 3p + 2$ for nonnegative integer p, such that their unperturbed energy spectra are gapless.[33,38,39,56] Figure 5 presents the energy spectrum of an armchair GNR for $U_0 = 1$ and $W = 80$ and 41, respectively, in Figs. 5(a) and 5(b). The same spectrum occurs around another Dirac cone at $k_y = \sqrt{3}K_0/2$. Edge-state branches are the isolated branches separated from the GNR subbands. The GNR subbands open up an energy interval between them, at the Dirac cone, leaving room for the edge-state branches to develop. This is seen more clearly in Figs. 5(a′) and 5(b′), where smaller k_y ranges are shown. The gray areas are the continuum spectrum for the bulk graphene, given by Eq. (6). States with energy $E(k_y)$ that falls outside the gray area should have their wave function exhibiting exponential behavior. Guided by this, the GNR subbands and the edge-state branches

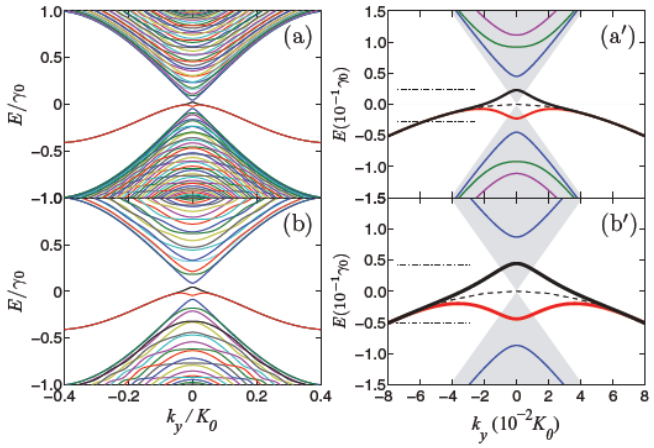

FIG. 5. (Color online) Energy spectrum of armchair GNR for $U_0 = 1$, and $W = 80$ in (a) and 41 in (b). Smaller k_y ranges are shown in (a′) and (b′), where gray areas are the continuum spectrum for the bulk graphene. Two branches outside the gray areas are edge-state branches: odd (even) parity for the upper (lower) branch. Dotted curve between the edge-state branches is that for a single open boundary. Horizontal (dotted-dashed) line segments in (a′) and (b′) denote energies to be considered in Fig. 6.

are easily identified. Furthermore, the edge states have two branches with the upper (lower) branch having odd (even) parity. This results from hybridizations between edge states on the two GNR edges. The fact that the edge-state branch for an open boundary, denoted by the dotted curve, is centrally positioned in energy between the two edge-state branches demonstrates a degenerate splitting feature, and it indicates that the edge states are pretty well formed. When the two branches overlap in energy, for sufficiently large k_y, the edge states on the two GNR edges become decoupled. It is worth pointing out that when the small k_y region of the edge-state branches falls within the gray area, their spatial profiles $|\Psi^{(\mathrm{NR})}_{\mathrm{A/B}}|^2$, on the A or B sites, are expected to exhibit bulklike characteristics. This is found in Fig. 6. When the edge-state branches overlap, linear superpositions of the even- and odd-parity wave functions produce edge-state wave functions $\Psi^{(\mathrm{NR})}_{\mathrm{R\,(L)}}$ that localize on the right (left) edges. These are shown in Figs. 6(a) and 6(b) for, respectively, the cases of $E = -0.03$, and -0.05.

Another important indication shown in Fig. 6 concerns the out-of-plane pseudospin for the edge states. The $|\Psi^{(\mathrm{NR})}_{\mathrm{A}}|^2$ and $|\Psi^{(\mathrm{NR})}_{\mathrm{B}}|^2$ curves fall exactly on top of one another in Fig. 6. This implies that the out-of-plane pseudospin vanishes for the edge states. Furthermore, the out-of-plane pseudospins of the GNR subbands are also found to be zero. We think that this is due to the highly symmetric alignment of the GNR edges. For less symmetric graphene boundary configurations, however, the edge-potential-induced out-of-plane pseudospin feature is expected to manifest near an armchair open boundary. This is left for further investigation.

We present in Fig. 7 the evolution of the two edge-state branches with the increase of U_0. For positive U_0, the edge-state branches are being drawn from the two highest GNR valence subbands. Meanwhile, an energy gap is formed which is increasing with U_0, and is indicated by Δ_p in Fig. 7(c). The gap is formed between two odd-parity branches, namely the GNR subband, denoted by $E^{\mathrm{odd}}_{\mathrm{bulk}}$, and the edge-state branch, denoted by $E^{\mathrm{odd}}_{\mathrm{edge}}$. On the other hand, there is an energy window in the spectrum that consists of only edge states. For example, in Fig. 7(c), the energy window, bounded by the $k_y = 0$ edge-state branch (even parity) and its neighboring GNR subband, on the lower energy side, is of the order of $0.02\gamma_0$.

C. Edge-potential-induced gap modulation

In this subsection, the edge-potential-induced energy gap $\Delta_p(U_0)$ is obtained up to second order in U_0^2. Toward this end, we consider $k_y = 0$. Equation (5) gives us $C^{(1)}_{\mathbf{k}_\alpha} = C^{(1)}_{\mathbf{k}_\beta} =$

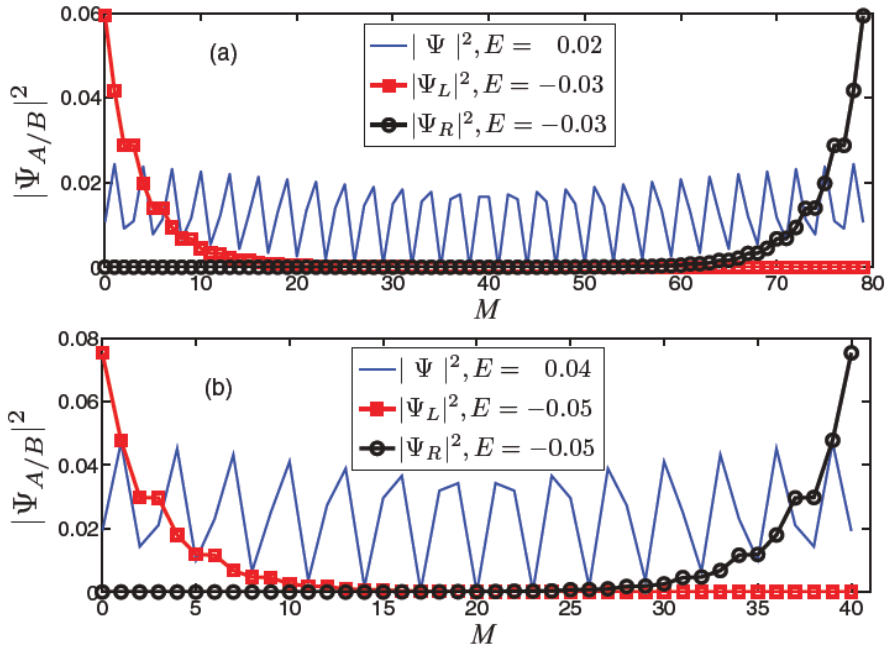

FIG. 6. (Color online) Wave-function spatial profiles for selected energies on the edge-state branches in Fig. 5. $W = 80$ in (a) and 41 in (b). Energies outside (inside) the gray areas in Fig. 5 exhibit edgelike (bulklike) profiles, denoted by squares and circles (solid curves). $\Psi_{\mathrm{R\,(L)}}$ denote wave functions that localize on the right (left) edges.

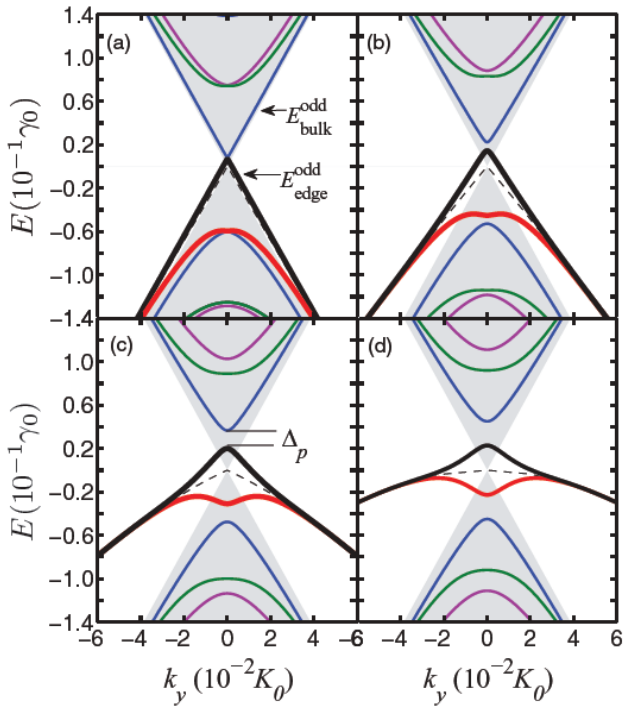

FIG. 7. (Color online) Energy spectrum of the $W = 80$ armchair GNR in Fig. 5. $U_0 = 0.2$, 0.5, 0.8, and 1.0 in (a), (b), (c), and (d), respectively. Near the Dirac cone, the GNR subband ($E^{\text{odd}}_{\text{bulk}}$) and the edge-state branch ($E^{\text{odd}}_{\text{edge}}$) are both of odd parity, as denoted in (a). The U_0-induced energy gap Δ_p is indicated in (c). Dotted curve is the open-boundary edge-state branch.

$C^{(1)}_{\mathbf{k}_\gamma} = 1/\sqrt{2}$, $C^{(2)}_{\mathbf{k}_\alpha} = C^{(2)}_{\mathbf{k}_\beta} = -\xi\eta/\sqrt{2}$, and $C^{(2)}_{\mathbf{k}_\gamma} = -C^{(2)}_{\mathbf{k}_\alpha}$ for $\alpha = (\xi,\eta)$. Substituting these into Eq. (26), we obtain $r_{2\alpha} = 0$ and

$$r_{1\alpha} = -\frac{e^{-ik_{\alpha x}M_w a/2}[-U_0\,\xi\eta + e^{-ik_{\alpha x}a_{2x}}]}{e^{ik_{\alpha x}M_w a/2}[-U_0\,\xi\eta + e^{ik_{\alpha x}a_{2x}}]}. \tag{27}$$

Energies for the odd-parity states are determined from Eq. (25), which in turns gives the equation $1 + r_{1\alpha} = 0$. For our purposes here, the unperturbed wave vector k_x for these states is at ηK when $U_0 = 0$. Keeping up to the second order in U_0, the correction $\delta k_{\alpha x}$ is,

$$\begin{aligned}\delta k_{\alpha x} &= \xi\Gamma_1 U_0 + \eta\Gamma_2 U_0^2\\ \Gamma_1 &= -\frac{1}{\sqrt{3}\,(p+1)},\\ \Gamma_2 &= \frac{1}{\sqrt{3}}\left[\frac{1}{2\,(p+1)} - \frac{1}{3(p+1)^2}\right].\end{aligned} \tag{28}$$

The energy shift δE_α, up to second order in δk_x, is obtained from Eq. (6), given by

$$\delta E_\alpha = -\xi\left(\sqrt{3}\,\delta k_{x,\alpha} - \tfrac{1}{2}\eta\,\delta k_{\alpha x}^2\right). \tag{29}$$

Substituting Eq. (28) into Eq. (29), the band edges of the subband $E^{\text{odd}}_{\text{bulk}}$, where $\eta = -1$, and the edge-state branch $E^{\text{odd}}_{\text{ed}}$, where $\eta = 1$, are obtained as

$$\delta E_\alpha = \left[\frac{1}{(p+1)}U_0 - \xi\eta\frac{p}{2(p+1)^2}U_0^2\right]. \tag{30}$$

Here $\xi = 1$. Finally, the energy gap Δ_p, up to second order in U_0, is obtained as

$$\Delta_p = E^{\text{odd}}_{\text{bulk}}(0) - E^{\text{odd}}_{\text{ed}}(0) = \frac{p}{(p+1)^2}U_0^2. \tag{31}$$

IV. CONDUCTANCE OF AN ARMCHAIR GNR

In this section, we present the conductance G of an armchair GNR and its dependences on the edge potential U_0 and the chemical potential μ of the GNR. Our major interest here is to identify the signatures of the edge states and the gap opening in the $G(U_0,\mu)$ characteristics. The Landauer-Büttiker formula[57,58] is used for the calculation of G.

Figure 8 shows the contour plot of G, where its value, in units of $2e^2/h$, is depicted by integers in the respective regions in the μ-U_0 plane. Essentially the integers denote the number of propagating (right-going) channels in the GNR. The $G = 0$ (black) region indicates the energy gap in μ, which has a zero μ interval at U_0 and opens up monotonically with U_0. The μ interval in the small U_0 regime is described by Eq. (31). Furthermore, the $U_0 = 0$ results can be understood by comparing the energy spectrum close to that in Fig. 7(a). Increasing μ from zero, there are two right-going channels, one from each Dirac cone, at $k_y = 0$ and $k_y = \sqrt{3}\,K_0/2$, giving $G = 2$. As μ increases further, approaching 0.07, two higher GNR subbands enter for each Dirac cone, and $G = 6$. On the other hand, decreasing μ from zero, the higher GNR subbands enter in a pair for each Dirac cone, and G's value is in the sequence 2, 6, and 8.

Similarly, the trend for finite U_0 can be understood from the energy spectrum for $U_0 = 1$, as shown in Fig. 7(d). A few

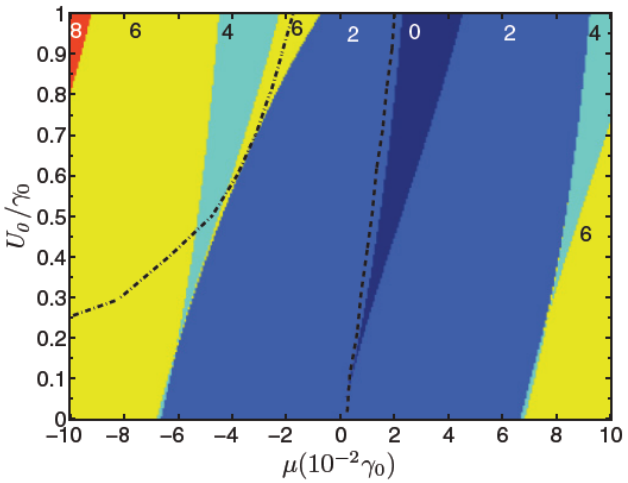

FIG. 8. (Color online) Dependences of conductance on the edge potential U_0 and the chemical potential μ. The armchair GNR has $W = 80$. Integers in the figure denote the conductance G, in units of $2e^2/h$, in the respective region. Dotted (dotted-dashed) line depicts the odd- (even-) parity edge-state branch that emerges from the continuum spectrum of the bulk graphene.

added features should be noted here. Higher GNR subbands are split and no longer enter in a pair as μ changes. The energy gap ($G = 0$) is shifted to the positive-μ region, and the splitting of the edge-state branches near a Dirac cone brings about interesting G structures. The conditions under which the edge-state branches emerge from the continuum spectrum are indicated by the dotted and dot-dashed lines. Thus increasing μ from zero, the G values are in the sequence 2, 0, 2, and 4. In the opposite direction, when μ decreases from zero, the sequence of G values becomes 2, 6, 4, 6, and 8. In between the dotted and the dot-dashed lines, where $G = 2$ and 6, the edge states, including both coupled and decoupled edge states, are the sole contributors to G. The jump from $G = 2$ to 6 arises from two (one) channels in the even- (odd-) parity edge-state branch, per Dirac cone. The next region ($G = 4$) is another region where G is contributed from edge states alone. Here, however, only decoupled edge states are involved. The characteristics presented above remain intact for the edge potential with a smooth spatial profile.[59] It is perhaps not unexpected that the atomic-scale profile for the edge potential is not very crucial for the features found in this work. It may be that it is the intravalley (small momentum change) scattering, rather than the intervalley (large momentum change) scattering, that must be invoked here. Finally, the edge-state features are expected to be robust against weak disorder due to their chiral nature.

V. CONCLUSIONS

In conclusion, we have studied the effects of edge potentials on an armchair graphene open boundary, and on armchair GNRs. The connection of the formation of the edge states with the edge-potential-induced pseudospin flipping at the open boundary has been elucidated. The subsequent generation of out-of-plane pseudospin polarizations at an open boundary is demonstrated. In the case of an armchair GNR, both the formation of edge states and the opening of an energy gap are found. These effects exhibit distinct characteristics in the conductance of the GNR. Finally, the edge-potential configuration considered in this work could be realized with the technique of anisotropic etching of graphene by thermally activated nickel nanoparticles,[52] with some of the etched graphene functioning as gating electrodes and others as the GNR.

ACKNOWLEDGMENTS

We acknowledge useful discussions with M. Monteverde, and we are grateful to him for referring us to Ref. 51. This work was supported by Taiwan NSC (Contract No. 100-2112-M-009-019), NCTS Taiwan, and a MOE-ATU grant.

[1] K. S. Novoselov, A. K. Geim, S. V. Morozov, D. Jiang, Y. Zhang, S. V. Dubonos, I. V. Grigorieva, and A. A. Firsov, Science **306**, 666 (2004).
[2] K. S. Novoselov, D. Jiang, F. Schedin, T. J. Booth, V. V. Khotkevich, S. V. Morozov, and A. K. Geim, Proc. Natl. Acad. Sci. USA **102**, 10451 (2005).
[3] A. K. Geim and K. S. Novoselov, Nat. Mater. **6**, 183 (2007).
[4] C. W. J. Beenakker, Rev. Mod. Phys. **80**, 1337 (2008).
[5] A. H. Castro Neto, F. Guinea, N. M. R. Peres, K. S. Novoselov, and A. K. Geim, Rev. Mod. Phys. **81**, 109 (2009).
[6] N. M. R. Peres and R. M. Ribeiro, New J. Phys. **11**, 095002 (2009).
[7] D. Abergel, V. Apalkov, J. Berashevich, K. Ziegler, and T. Charkraborty, Adv. Phys. **59**, 261 (2010).
[8] S. DasSarma, S. Adam, E. H. Hwang, and E. Ross, Rev. Mod. Phys. **83**, 407 (2011).
[9] P. Avouris, Z. Chen, and V. Perebeinos, Nat. Nanotech. **2**, 605 (2007).
[10] F. Miao, S. Wijeratne, Y. Zhang, U. C. Coskun, W. Bao, and C. N. Lau, Science **317**, 1530 (2007).
[11] L. A. Ponomarenko, F. Schedin, M. I. Katsnelson, R. Yang, E. W. Hill, K. S. Novoselov, and A. K. Geim, Science **320**, 356 (2008).
[12] F. Schwierz, Nat. Nanotech. **5**, 487 (2010).
[13] Y. W. Son, M. L. Cohen, and S. G. Louie, Nature (London) **444**, 347 (2006).
[14] X. Wang, Y. Ouyang, X. Li, H. Wang, J. Guo, and H. Dai, Phys. Rev. Lett. **100**, 206803 (2008).
[15] M. I. Katsnelson, K. S. Novoselov, and A. K. Geim, Nat. Phys. **2**, 620 (2006).
[16] K. I. Bolotin, K. J. Sikes, Z. Jiang, M. Klima, G. Fudenberg, J. Hone, P. Kim, and H. L. Stormer, Solid State Commun. **146**, 351 (2008).
[17] A. A. Balandin, S. Ghosh, W. Z. Bao, I. Calizo, D. Teweldebrhan, F. Miao, and C. N. Lau, Nano Lett. **8**, 902 (2008).
[18] C. H. Park, Y. W. Son, L. Yang, M. L. Cohen, and S. G. Louie, Nano Lett. **8**, 2920 (2008).
[19] L. Majidi and M. Zareyan, Phys. Rev. B **83**, 115422 (2011).
[20] M. Mecklenburg and B. C. Regan, Phys. Rev. Lett. **106**, 116803 (2011).
[21] A. Rycerz, J. Tworzydło, and C. W. J. Beenakker, Nat. Phys. **3**, 172 (2007).
[22] J. L. Garcia-Pomar, A. Cortijo, and M. Nieto-Vesperinas, Phys. Rev. Lett. **100**, 236801 (2008).
[23] D. Gunlycke and C. T. White, Phys. Rev. Lett. **106**, 136806 (2011).
[24] A. F. Young and P. Kim, Nat. Phys. **5**, 222 (2009).
[25] N. Stander, B. Huard, and D. Goldhaber-Gordon, Phys. Rev. Lett. **102**, 026807 (2009).
[26] K. S. Novoselov, A. K. Geim, S. V. Morozov, D. Jiang, M. I. Katsnelson, I. V. Grigorieva, S. V. Dubonos, and A. A. Firsov, Nature (London) **438**, 197 (2005).
[27] Y. Zhang, J. W. Tan, H. L. Stormer, and P. Kim, Nature (London) **438**, 201 (2005).
[28] H. Suzuura and T. Ando, Phys. Rev. Lett. **89**, 266603 (2002).
[29] E. McCann, K. Kechedzhi, V. I. Fal'ko, H. Suzuura, T. Ando, and B. L. Altshuler, Phys. Rev. Lett. **97**, 146805 (2006).
[30] A. F. Morpurgo and F. Guinea, Phys. Rev. Lett. **97**, 196804 (2006).
[31] V. V. Chelanov, V. Fal'ko, and B. L. Altshuler, Science **315**, 1252 (2007).
[32] S. E. Stein and R. L. Brown, J. Am. Chem. Soc. **109**, 3721 (1987).
[33] M. Fujita, K. Wakabayashi, K. Nakada, and K. Kusakabe, J. Phys. Soc. Jpn. **65**, 1920 (1996).

[34]K. Nakada, M. Fujita, G. Dresselhaus, and M. S. Dresselhaus, Phys. Rev. B **54**, 17954 (1996).
[35]S. Ryu and Y. Hatsugai, Phys. Rev. Lett. **89**, 077002 (2002).
[36]T. Hikihara, X. Hu, H. H. Lin, and C. Y. Mou, Phys. Rev. B **68**, 035432 (2003).
[37]C. L. Kane and E. J. Mele, Phys. Rev. Lett. **95**, 226801 (2005).
[38]M. Ezawa, Phys. Rev. B **73**, 045432 (2006).
[39]L. Brey and H. A. Fertig, Phys. Rev. B **73**, 235411 (2006).
[40]N. M. R. Peres, A. H. Castro Neto, and F. Guinea, Phys. Rev. B **73**, 195411 (2006).
[41]N. M. R. Peres, F. Guinea, and A. H. Castro Neto, Phys. Rev. B **73**, 125411 (2006).
[42]C. Ritter, S. S. Makler, and A. Latgé, Phys. Rev. B **77**, 195443 (2008).
[43]W. Yao, S. A. Yang, and Q. Niu, Phys. Rev. Lett. **102**, 096801 (2009).
[44]K. Wakabayashi, S. Okada, R. Tomita, S. Fujimoto, and Y. Natsume, J. Phys. Soc. Jpn. **79**, 034706 (2010).
[45]S. Bhowmick and V. B. Shenoy, Phys. Rev. B **82**, 155448 (2010).
[46]K. Wakabayashi, K. Sasaki, T. Nakanishi, and T. Enoki, Sci. Technol. Adv. Mater. **11**, 054504 (2010).
[47]W. Apel, G. Pal, and L. Schweitzer, Phys. Rev. B **83**, 125431 (2011).
[48]C. Tao, L. Jiao, O. V. Yazyev, Y. C. Chen, J. Feng, X. Zhang, R. B. Capaz, J. M. Tour, A. Zettl, S. G. Louie, H. Dai, and M. F. Crommie, Nat. Phys. **7**, 616 (2011).
[49]P. Delplace, D. Ullmo, and G. Montambaux, Phys. Rev. B **84**, 195452 (2011).
[50]J. Wurm, K. Richter, and I. Adagideli, Phys. Rev. B **84**, 075468 (2011).
[51]X. Jia, M. Hofmann, V. Meunier, B. G. Sumpter, J. Campos-Delgado, J. M. Romo-Herrera, H. Son, Y. P. Hsieh, A. Reina, J. Kong, M. Terrones, and M. S. Dresselhaus, Science **323**, 1701 (2009).
[52]L. C. Campos, V. R. Manfrinato, J. D. Sanchez-Yamagishi, J. Kong, and P. Jarillo-Herrero, Nano Lett. **9**, 2600 (2009).
[53]I. Martin, Y. M. Blanter, and A. F. Morpurgo, Phys. Rev. Lett. **100**, 036804 (2008).
[54]Edge states were obtained in recent work (Ref. 44) on the chemical modification of an armchair edge into a Klein edge, and with a finite transfer integral between Klein's bonds and the armchair edge.
[55]I. Tamm, Phys. Z. Sowjetunion **1**, 733 (1932).
[56]Y. W. Son, M. L. Cohen, and S. G. Louie, Phys. Rev. Lett. **97**, 216803 (2006).
[57]R. Landauer, Philos. Mag. **21**, 863 (1970).
[58]M. Buttiker, Phys. Rev. Lett. **57**, 1761 (1986).
[59]C. H. Chiu and C. S. Chu (unpublished).

Nonuniversality of the intrinsic inverse spin-Hall effect in diffusive systems

L. Y. Wang,[1] A. G. Mal'shukov,[2] and C. S. Chu[1,3]
[1]Department of Electrophysics, National Chiao Tung University, Hsinchu 30010, Taiwan
[2]Institute of Spectroscopy, Russian Academy of Sciences, 142190 Troitsk, Moscow oblast, Russia
[3]National Center for Theoretical Sciences, Physics Division, Hsinchu 30043, Taiwan
(Received 21 November 2011; revised manuscript received 16 March 2012; published 2 April 2012)

We studied the electric current induced in a two-dimensional electron gas by the spin current, in the presence of Rashba and cubic Dresselhaus spin-orbit interactions. We found out that the factor relating the electric and spin currents is not universal, but rather depends on the origin of the spin current. Drastic distinction has been found between two cases: the spin current created by diffusion of an inhomogeneous spin density, and the pure homogeneous spin current. We found that in the former case the inverse spin-Hall effect electric current is finite, while it turns to zero in the latter case, if the spin-orbit coupling is represented by Rashba interaction.

DOI: 10.1103/PhysRevB.85.165201 PACS number(s): 72.25.Dc, 71.70.Ej, 75.76.+j

I. INTRODUCTION

The spin-Hall effect (SHE) and the inverse spin-Hall effect (ISHE) can be observed in two- and three-dimensional electron systems with a strong enough spin-orbit interaction (SOI).[1,2] Via this interaction the electric current induces a flux of spin polarization flowing in the perpendicular direction and vice versa. These effects take place in metals and semiconductors, where the spin-orbit interaction arises from impurity scattering, or band structure effects. Nowadays they are being intensively studied theoretically (for a review see Ref. 3) and experimentally.[4,5] These phenomena establish an important connection between spin and charge degrees of freedom that can be employed in spintronic applications.

Here we will focus on ISHE. This effect is driven by the spin current which can be produced in different ways. It can be created by diffusion of an inhomogeneous spin polarization, or it can be induced directly by a motive force of various natures.[6,7] In experimental studies the former method was used in Refs. 5,8, while the latter was employed in Refs. 9,10. From the theoretical point of view there are two quite distinct mechanisms of ISHE, depending on the extrinsic or intrinsic nature of SOI in an electron system. The extrinsic effect is promoted by the spin-orbit scattering of electrons from impurities.[2] The intrinsic effect is associated with the spin-orbit splitting of electron energy bands. This effect has been studied in Ref. 11 together with the extrinsic mechanism. A surprising result of this study is that the finite inverse SHE takes place even in the case of a pure intrinsic Rashba[12] SOI, while the direct effect has been shown to vanish in the considered case of a diffusive system.[13] A reasonable explanation is that the Onsager relation between direct (SHE) and reciprocal (ISHE) effects should not be satisfied, because the spin-current is not conserving. This argument also means that for the ISHE effect the coefficient in the local linear dependence $I_c = \mathcal{C} I_s$ of the charge current density I_c from the spin current density I_s can depend on the source that originally excites I_s. In this sense ISHE is not universal. At the same time, SHE is a universal effect, because the coefficient relating I_s to I_c does not depend on how the electric current is produced. It can be created, for example, by electron diffusion, as well as by an external electric field. The result will be the same. It follows from the gage invariance of the electromagnetic field. Formally, one obtains the same spin current, independent of whether it is induced by the scalar electric potential or time-dependent vector potential.

In order to demonstrate the nonuniversality of ISHE we will consider two kinds of spin-current sources. In the first case, an inhomogeneous spin polarization parallel to the z axis creates the spin flux due to spin diffusion. In the second case, the spin current is driven by a spatially uniform "electric" field, such that the fields acting on up and down spins have opposite signs. The latter situation corresponds to spin current generation mechanisms suggested in Refs. 6,7. Our goal is to show that the factors $\mathcal{C}$ are different in these two situations. Since our analysis has shown that in the case of the Rashba spin-orbit interaction $\mathcal{C} = 0$ for the source of the second kind, we will consider the cubic Dresselhaus interaction, as well, and demonstrate that the Onsager relation holds in this case.

The outline of the paper is as follows. In Sec. II the linear response equations relating the spin and charge currents to the auxiliary fields will be written for a disordered two-dimensional degenerate electron gas (2DEG). From this pair of equations the auxiliary fields can be excluded and linear relations between the electric and spin currents can be established. In Sec. III this theory will be applied to the cases with Rashba (Sec. III A) and Dresselhaus (Sec. III B) spin-orbit couplings. The discussion of results will be presented in Sec. IV.

II. LINEAR RESPONSE THEORY

The Hamiltonian of the electron system has the form

$$H = H_0 + V, \tag{1}$$

where H_0 is the unperturbed Hamiltonian of the 2DEG, which includes the electrons' spin-orbit coupling and their scattering on randomly distributed spin-independent elastic scatterers. The spin-orbit coupling has the general form

$$H_{so} = \mathbf{h_k} \cdot \boldsymbol{\sigma}, \tag{2}$$

where the effective magnetic field $\mathbf{h_k}$ is a function of the electron momentum $\mathbf{k}$ and $\boldsymbol{\sigma} = (\sigma_x, \sigma_y, \sigma_z)$ is the vector of Pauli matrices. In general, $\mathbf{h_k}$ can be generated by the bulk-inversion asymmetry in the bulk and structure-inversion asymmetry in a quantum well (QW).[14] The perturbation term $V = V_1 + V_2$

represents interactions of electrons with the auxiliary fields. We will consider two types of fields. The first one is a slowly varying in time nonuniform Zeeman field B which is directed perpendicular to the 2DEG (z direction). The corresponding interaction Hamiltonian is

$$V_1 = \sigma_z B. \tag{3}$$

Another interaction is

$$V_2 = \sigma_z \mathbf{k} \cdot \mathbf{A}. \tag{4}$$

This Hamiltonian contains the uniform spin-dependent field $\sigma_z \mathbf{A}$, where $\mathbf{A}$ slowly varies in time. Such a field induces the spin current by driving in opposite directions electrons having opposite spins. It can be created, for example, by applying a time-dependent strain to a noncentrosymmetric semiconductor. Indeed, as known[15] the strain field u_{xz} gives rise to the spin-orbit interaction $\alpha \sigma_z u_{xz} k_x$. Hence, in this case $A_x = \alpha u_{xz}$. Other mechanisms[6,7] of creating homogeneous spin currents can also be presented in a form of a spin-dependent vector potential that is able to drive spins.

Within the linear response theory the spin I^s and charge I^c currents of noninteracting electrons can be written in terms of retarded $G^r_{\mathbf{k},\mathbf{k}'}(\omega)$ and advanced $G^a_{\mathbf{k},\mathbf{k}'}(\omega)$ single-particle Green's functions. Due to impurity scattering these functions are nondiagonal with respect to the wave vectors $\mathbf{k}$ and $\mathbf{k}'$. The linear response expressions for the currents, as functions of the frequency Ω and wave vector $\mathbf{q}$, at $\Omega \to 0$ are given by

$$\begin{aligned}\mathbf{I}^{s/c}(\Omega,\mathbf{q}) = -i \sum_{\mathbf{k},\mathbf{k}'} \int \frac{d\omega}{2\pi} \langle \mathrm{Tr}\{ &\left[G^r_{\mathbf{k},\mathbf{k}'}(\omega) - G^a_{\mathbf{k},\mathbf{k}'}(\omega)\right] \mathbf{j}_{s/c} G^a_{\mathbf{k}'+\mathbf{q},\mathbf{k}+\mathbf{q}}(\omega+\Omega) V(\Omega,\mathbf{q}) n_F(\omega) \\ &+ G^r_{\mathbf{k},\mathbf{k}'}(\omega) \mathbf{j}_{s/c} \left[G^r_{\mathbf{k}'+\mathbf{q},\mathbf{k}+\mathbf{q}}(\omega+\Omega) - G^a_{\mathbf{k}'+\mathbf{q},\mathbf{k}+\mathbf{q}}(\omega+\Omega)\right] V(\Omega,\mathbf{q}) n_F(\omega+\Omega) \} \rangle \\ &+ \frac{1}{2} \sum_{\mathbf{k}} n_F(E_{\mathbf{k}}) \mathrm{Tr} \left[\tau_{s/c}, \frac{\partial V(\Omega,\mathbf{q})}{\partial \mathbf{k}}\right]_+ ,\end{aligned} \tag{5}$$

where the spin-current and charge-current operators have the conventional form[16] $\mathbf{j}_{s/c} = (1/2)[\tau_{s/c}, \mathbf{v}]_+$, with $\mathbf{v} = \mathbf{k}/m^* + \partial(\mathbf{h}_\mathbf{k} \cdot \boldsymbol{\sigma})/\partial \mathbf{k}$ and $\tau_s = \sigma_z$, $\tau_c = e$; $n_F(\omega)$ is the Fermi distribution. In the following the low-temperature case will be assumed, so that $n_F(\omega + \Omega) \simeq n_F(\omega) - \Omega \delta(\omega)$. The angular brackets denote averaging over disorder. This averaging will be performed within the semiclassic approximation, according to the standard procedure,[17] where we will neglect the weak-localization corrections. We will assume that the spatial variations of the external field are slow within the electron mean-free path l, so that $lq \ll 1$. This case corresponds to the diffusion approximation, implying the expansion of Eq. (5) in powers of q. Also the SOI field will be assumed weak enough that $h_{k_F} \ll 1/\tau$, where τ is the mean electron scattering time.

III. INVERSE SPIN-HALL EFFECT

A. Rashba SOI

Let us first consider ISHE in the case of Rashba spin-orbit interaction, where the spin-orbit field is linear in k and has the form $\mathbf{h}_\mathbf{k} \equiv \mathbf{h}^R_\mathbf{k} = \alpha \mathbf{k} \times \hat{z}$. If the auxiliary field is V_1, given by Eq. (3), it creates a nonequilibrium and nonuniform in space spin polarization S_z. This distribution of electron spins relaxes to the uniform state via diffusion that is accompanied by a pure spin current. When $V(\Omega,\mathbf{q})$ in Eq. (5) is represented by $V_1(\Omega,\mathbf{q})$, the last term in this expression vanishes. Also, the terms containing the products $G^r G^r$ and $G^a G^a$ can be shown to vanish, at least up to linear in q terms. Since in the following the higher-order terms starting from q^2 will be ignored, only the products of the form $G^r G^a$ will be retained in Eq. (5). We assume that B in Eq. (3) varies in the x direction, so that I^c is expected to flow in the y direction. In Fig. 1 the Feynman diagrams contributing to Eq. (5), where $V = V_1$, are shown. The upper (lower) arms in the diagrams denote the impurity averaged functions $G^{r(a)}_\mathbf{k}(\omega) = (\omega - E_\mathbf{k} - \mathbf{h}_\mathbf{k} \cdot \boldsymbol{\sigma} \pm i\Gamma)^{-1}$ and the dashed lines depict the random scattering potential correlator $\langle |U_\mathbf{k}|^2 \rangle$. For simplicity this correlator will be assumed short-ranged, i.e., independent of k, so that $\Gamma = \pi N_F \langle |U_\mathbf{k}|^2 \rangle \equiv \pi N_F |U|^2 = 1/2\tau$ is simply a constant. The multiple scattering blocks in the diagrams shown in Figs. 1(b) and 1(d) represent processes where the initial electron spin density S_z evolves in the diffusion process to S_i. Since this process is accompanied by the spin precession due to Rashba SOI, i can be either z or x, as follows from the spin diffusion equation[18] for the spin polarization varying in space along the x coordinate. In general such a diffusion-precession dynamics

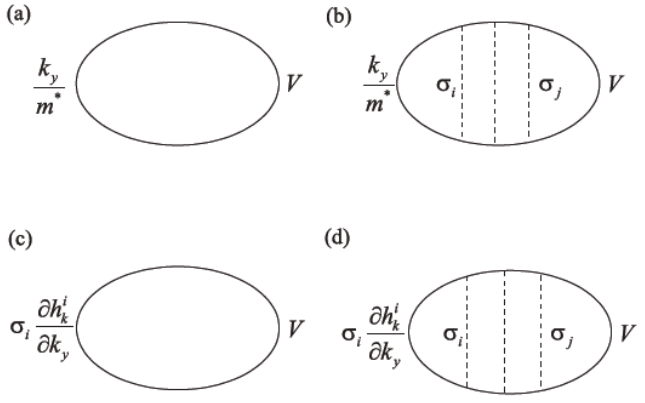

FIG. 1. The Feynman diagrams for the charge current generated by the intrinsic spin-Hall effect. The auxiliary field V can be either V_1 or V_2, where V_1 and V_2 are defined by Eq. (3) and Eq. (4), respectively.

is represented by the diffusion propagator $D_{ij}(\mathbf{q})$. In the matrix form it can be represented as

$$D_{ij} = [(1 - |U|^2\Psi/2)^{-1}]_{ij}\,, \tag{6}$$

$$\Psi_{ij} = \sum_{\mathbf{k}} \mathrm{Tr}\big[\sigma_i G^r_{\mathbf{k}+\mathbf{q}}(\omega)\sigma_j G^a_{\mathbf{k}}(\omega)\big]. \tag{7}$$

Using the above definition, the contribution of all four types of diagrams in Fig. 1 can be written as

$$I^c_y = i\frac{\Omega}{2\pi}B\left(K_{yz}D_{zz} + K_{yx}D_{xz} + \alpha\frac{2\pi N_F}{\Gamma}D_{xz}\right), \tag{8}$$

where

$$K_{ij} = \sum_{\mathbf{k}} \frac{k_i}{m^*}\mathrm{Tr}\big[G^r_{\mathbf{k}+\mathbf{q}}(\omega)\sigma_j G^a_{\mathbf{k}}(\omega)\big]. \tag{9}$$

It is easy to see that the diagonal components of D are finite at $q \to 0$, while the nondiagonal ones vanish as the first power of q. Therefore, in the leading approximation the correlator K in the second term of Eq. (8) must be calculated at $q = 0$. Up to the small semiclassic corrections of the order of $(\alpha k_F/E_F)^3$ this correlator is $K_{yx} = -2\pi\alpha N_F/\Gamma$, and the last two terms cancel each other. At the same time, it is easy to see that K_{yy} is 0 at $q = 0$. Therefore, we did not include the corresponding term $K_{yy}D_{yz}$ into Eq. (8). Further, as follows from Eq. (9), the correlator K_{yz} is proportional to $\mathbf{h_k} \times \mathbf{h_{k+q}}$. Therefore, it turns to 0 at $q = 0$. In the leading approximation one finds from Eqs. (8) and (9) that $K_{yz} = -i\pi q\alpha^2 N_F k_F^2/2m^*\Gamma^3$ and

$$I^c_y = \frac{\Omega}{2\pi}qBD_{zz}\frac{\alpha^2k_F^2}{4\Gamma^3}. \tag{10}$$

Our goal is to get an expression of the charge current through the spin current I^s_x. Therefore, the next step is to calculate the spin current induced by the perturbation $B\sigma_z$. This current can be written in the form

$$I^s_x = i\frac{\Omega}{2\pi}B\left(R^x_{zx}D_{xz} + D_{zz}\sum_{\mathbf{k}}\frac{k_x}{m^*}\mathrm{Tr}\big[\sigma_z G^r_{\mathbf{k}+\mathbf{q}}(\omega)\sigma_z G^a_{\mathbf{k}}(\omega)\big]\right), \tag{11}$$

where

$$R^i_{jk} = \sum_{\mathbf{k}}\frac{k_i}{m^*}\mathrm{Tr}\big[\sigma_j G^r_{\mathbf{k}+\mathbf{q}}(\omega)\sigma_k G^a_{\mathbf{k}}(\omega)\big]. \tag{12}$$

The second term in the large parentheses of Eq. (11) is equal to $-i\pi N_F q v_F^2 D_{zz}/2\Gamma^2$. This term represents the diffusion spin current. In its turn the first term is associated with spin precession caused by the Rashba field. It takes a simple form in the case when $q \ll \alpha m^*$, that is, when spatial variations of the Zeeman field are slower than spin-density variations caused by spin precession in the SOI field. In this case it follows from Eq. (6) that $D_{xz} = |U|^2\Psi_{xz}D_{xx}D_{zz}/2$. A straightforward calculation using Eqs. (6), (7), and (12) gives for the first term in the large parentheses of Eq. (11) the expression $i\pi N_F q v_F^2 D_{zz}/\Gamma^2$, which is twice larger and has opposite sign with respect to the second term. Finally, from Eqs. (10) and (11) the charge current becomes

$$I^c_y = -e\frac{\alpha^2 m^*}{\Gamma}I^s_x. \tag{13}$$

This result coincides with Ref. 11, taking into account that $2\Gamma = 1/\tau$ and that the definition of I^s_x in Ref. 11 differs by the factor 1/2.

The next example is the charge current induced in the y direction by the external perturbation given by Eq. (4), where $\mathbf{A}$ is parallel to the x axis. In this case the last term in Eq. (5) turns to zero, along with the terms containing the products G^rG^r and G^aG^a. Further, a simple inspection of diagram (a) in Fig. 1 shows that it is zero at $q = 0$. The contribution of other diagrams to I^c_y can be expressed as

$$I^c_y = i\frac{\Omega}{2\pi}A\sum_i\left(\frac{|U|^2}{2}K_{yi} + \frac{\partial h^i_{\mathbf{k}}}{\partial k_y}\right)D_{ii}R^x_{iz}, \tag{14}$$

where the first term corresponds to Fig. 1(b), while the second one is given by Figs. 1(c) and 1(d). Since $q = 0$, only diagonal components of D enter in Eq. (14). Also, at $q = 0$ only $i = x$ must be retained in the sum. As a result, after calculation of K_{yx}, one can see that the sum in the large parentheses turns into zero, up to the small semiclassic corrections of the order of $(\alpha k_F/E_F)^3$. Therefore, within the semiclassic approximation the homogeneous pure spin current cannot induce ISHE. At the same time the spin current created by this source is finite and is given by the Drude formula

$$I^s_x = im^*\Omega A\frac{v_F^2N_F}{2\Gamma}. \tag{15}$$

This expression does not depend on the spin-orbit coupling. The latter enters as a small correction $\sim h_k^2\tau^2$.

Our calculations in this subsection show that ISHE is not universal. The electric current induced by this effect is finite, or zero, depending on whether the spin-current is produced by diffusion of an inhomogeneous spin polarization or is a pure uniform spin flux created by an external force of the form Eq. (4). The driving force of this sort could be taken into account within the formalism employed in Ref. 19. We, however, cannot directly see whether their expressions for spin and charge currents give, as we expect, vanishing ISHE, because these equations are presented in a rather general form.

B. Dresselhaus SOI

Although at $V = V_2$ and for SOI given by the Rasha interaction the electric current is zero, we do not expect that the same takes place for a Dresselhaus SOI that is cubic in k. The reason is that the spin-Hall effect does not vanish in the latter case.[20] The Dresselhaus SOI field in a quantum well grown along the [001] direction is given by[21]

$$h^x_{\mathbf{k}} = \beta k_x\big(k_y^2 - \kappa_z^2\big), \quad h^y_{\mathbf{k}} = \beta k_y\big(\kappa_z^2 - k_x^2\big), \tag{16}$$

where κ_z^2 denotes the operator $-(\partial/\partial z)^2$ averaged over the lowest subband wave function. Since $h^i_{\mathbf{k}}$ is a nonlinear function of $\mathbf{k}$, $\nabla_{\mathbf{k}}h^i_{\mathbf{k}}$ entering into Eq. (14) is not a constant. Therefore Eq. (14) has to be modified. Denoting by a bar the average $\overline{\nabla_{\mathbf{k}}h^i_{\mathbf{k}}}$ over the Fermi surface, the modified expression for the

current can be written in the form

$$I_y^c = i\frac{\Omega}{2\pi}A\Big[\sum_i\left(\frac{|U|^2}{2}K_{yi}+\overline{\frac{\partial h_{\mathbf{k}}^i}{\partial k_y}}\right)D_{ii}R_{iz}^x + \frac{|U|^2}{2}\sum_i\Theta_i D_{ii}R_{iz}^x+\Phi\Big], \tag{17}$$

where

$$\Theta_i=\sum_{j\mathbf{k}}\left(\frac{\partial h_{\mathbf{k}}^j}{\partial k_y}-\overline{\frac{\partial h_{\mathbf{k}}^j}{\partial k_y}}\right)\mathrm{Tr}\big[\sigma_j G_{\mathbf{k}}^r(\omega)\sigma_i G_{\mathbf{k}}^a(\omega)\big] \tag{18}$$

and

$$\Phi=\sum_{ij\mathbf{k}}k_x\left(\frac{\partial h_{\mathbf{k}}^i}{\partial k_y}-\overline{\frac{\partial h_{\mathbf{k}}^i}{\partial k_y}}\right)\mathrm{Tr}\big[\sigma_j G_{\mathbf{k}}^r(\omega)\sigma_z G_{\mathbf{k}}^a(\omega)\big]. \tag{19}$$

It is easy to see that the first term in Eq. (17) turns to zero, similar to Eq. (14) in the Rashba case. However, other two terms are finite, while they vanish for Rashba SOI, as well as for any other SOI which depends linearly on $\mathbf{k}$. Taking SOI in the form of Eq. (16), from definitions (18), (19), (12), and (6)–(7) one obtains at $q=0$

$$\begin{aligned}
R_{yz}^x &= -2\pi\frac{N_F}{\Gamma^2}\overline{h_{\mathbf{k}}^x k_x}, \quad R_{xz}^x=0,\\
\Phi &= -2\pi\frac{N_F}{\Gamma^2}\left(\overline{\frac{\partial h_{\mathbf{k}}^y}{\partial k_y}h_{\mathbf{k}}^x k_x}-\overline{\frac{\partial h_{\mathbf{k}}^x}{\partial k_y}h_{\mathbf{k}}^y k_x}-\overline{\frac{\partial h_{\mathbf{k}}^y}{\partial k_y}}\,\overline{h_{\mathbf{k}}^x k_x}\right),\\
\Psi_{xx}&=\Psi_{yy}=\frac{2\pi N_F}{\Gamma}-\frac{\pi N_F}{\Gamma^3}\overline{h_{\mathbf{k}}^2},\\
D_{xx}&=D_{yy}=\frac{2\Gamma^2}{\overline{h_{\mathbf{k}}^2}}.
\end{aligned} \tag{20}$$

Since only R_{yz}^x is finite in Eq. (17), one has to calculate Θ_y. From Eq. (18) it can be expressed as

$$\Theta_y=\pi\frac{N_F}{\Gamma^3}\left(2\overline{\frac{\partial h_{\mathbf{k}}^x}{\partial k_y}h_{\mathbf{k}}^x h_{\mathbf{k}}^y}-2\overline{\frac{\partial h_{\mathbf{k}}^y}{\partial k_y}h_{\mathbf{k}}^{x2}}+\overline{\frac{\partial h_{\mathbf{k}}^y}{\partial k_y}}\,\overline{h_{\mathbf{k}}^2}\right). \tag{21}$$

Collecting all together one obtains from Eq. (17)

$$I_y^c = ieA\Omega\frac{N_F}{\Gamma^2}\Big[2\frac{\overline{h_{\mathbf{k}}^x k_x}}{\overline{h_{\mathbf{k}}^2}}\left(\overline{\frac{\partial h_{\mathbf{k}}^y}{\partial k_y}h_{\mathbf{k}}^{x2}}-\overline{\frac{\partial h_{\mathbf{k}}^x}{\partial k_y}h_{\mathbf{k}}^x h_{\mathbf{k}}^y}\right) + \overline{\frac{\partial h_{\mathbf{k}}^x}{\partial k_y}h_{\mathbf{k}}^y k_x}-\overline{\frac{\partial h_{\mathbf{k}}^y}{\partial k_y}h_{\mathbf{k}}^x k_x}\Big]. \tag{22}$$

This electric current can now be expressed through the spin current. The latter is induced by the time-dependent "vector potential" A in (4) and is given by (15). Denoting by Q the expression in the square brackets of Eq. (22), one obtains

$$I_y^c=\frac{2eQ}{\Gamma m^* v_F^2}I_x^s. \tag{23}$$

Taking into account that $Q\propto h_{\mathbf{k}}^2$ it easy to see that the charge-to-spin current ratio is of the same order of magnitude as in the case considered in Sec. III A, Eq. (13), provided that the Rashba and Dresselhaus interactions are comparable in their strengths. One more useful relation can be obtained by using the expression for the spin-Hall conductivity derived in Refs. 20,22. This conductivity can be written as $\sigma_{SH}=eN_F Q/\Gamma^2$. Expressing Q in Eq. (23) through σ_{SH}, and writing the electric conductivity in the form of the Einstein relation $\sigma=2N_F D$, we find

$$I_y^c=\frac{\sigma_{SH}}{\sigma}I_x^s. \tag{24}$$

On the other hand, the spin current induced by the spin-Hall effect is given by $I_x^s=\sigma_{SH}E$, where E is the electric field in the y direction. Writing it as $E=I_c^y/\sigma$ we arrive at $I_x^s=\sigma_{SH}I_y^c/\sigma$. This equation, together with Eq. (24), establishes Onsager relations between spin and charge currents.

IV. CONCLUSIONS

Our analysis shows that the proportionality coefficient in the linear relation between the electric and spin current densities in the inverse spin-Hall effect depends on the origin of the spin current. Therefore, it is not possible to introduce a universal parameter that determines a charge to spin current response. This nonuniversality is most clearly seen in the case of Rashba SOI, where a pure spin current produced by diffusion of an inhomogeneous spin polarization gives rise to the finite electric current, while the latter is zero when the spin current is induced by a force that is uniform in space. In this situation, however, the ISHE produces a finite charge current, if SOI is represented by a Dresselhaus SOI that is nonlinear in k. It is important that in such a case the spin-Hall effect and ISHE obey the Onsager relation for coefficients relating the spin and charge currents.

It should be noted that the expressions for the spin and charge currents calculated above are related to local current densities, while what is experimentally measured are total electric currents, or electric potentials that are responses not to local spin currents, but rather to currents that are integrated over some distance (in 2D transport). For example, due to SOI the spin-current density created by spin diffusion oscillates and decays when the distance x from the spin-injection source is increasing. One has to integrate this current over x to obtain the total electric current induced by ISHE. Since the relation Eq. (13) has the local form it will be preserved after such an integration.

ACKNOWLEDGMENTS

This work was supported by Taiwan NSC (Contract No. 100-2112-M-009-019), NCTS Taiwan, and a MOE-ATU grant.

[1] M. I. Dyakonov and V. I. Perel, Phys. Lett. A **35**, 459 (1971); S. Zhang, Phys. Rev. Lett. **85**, 393 (2000).

[2] J. E. Hirsch, Phys. Rev. Lett. **83**, 1834 (1999).

[3] H.-A. Engel, E. I. Rashba, and B. I. Halperin, in *Handbook of Magnetism and Advanced Magnetic Materials*, edited by H. Kronmüller and S. Parkin (Wiley, Chichester, UK, 2007).

[4]Y. K. Kato *et al.*, Science **306**, 1910 (2004); J. Wunderlich, B. Kaestner, J. Sinova, and T. Jungwirth, Phys. Rev. Lett. **94**, 047204 (2005).

[5]S. O. Valenzuela and M. Tinkham, Nature (London) **442**, 176 (2006); E. Saitoh, M. Ueda, H. Miyajima, and G. Tatara, Appl. Phys. Lett. **88**, 182509 (2006); T. Seki *et al.*, Nature Mater. **7**, 125 (2008); T. Kimura, Y. Otani, T. Sato, S. Takahashi, and S. Maekawa, Phys. Rev. Lett. **98**, 156601 (2007).

[6]A. G. Malshukov, C. S. Tang, C. S. Chu, and K. A. Chao, Phys. Rev. B **68**, 233307 (2003).

[7]R. D. R. Bhat and J. E. Sipe, Phys. Rev. Lett. **85**, 5432 (2000).

[8]J. Wunderlich *et al.*, e-print arXiv:0811.3486.

[9]L. K. Werake, B. A. Ruzicka, and Hui Zhao, Phys. Rev. Lett. **106**, 107205 (2011).

[10]H. Zhao, E. J. Loren, H. M. van Driel, and A. L. Smirl, Phys. Rev. Lett. **96**, 246601 (2006).

[11]P. Schwab, R. Raimondi, and C. Gorini, Europhys. Lett. **90**, 67004 (2010).

[12]Yu. A. Bychkov and E. I. Rashba, J. Phys. C **17**, 6039 (1984).

[13]J. I. Inoue, G. E. W. Bauer, and L. W. Molenkamp, Phys. Rev. B **70**, 041303 (2004); E. G. Mishchenko, A. V. Shytov, and B. I. Halperin, Phys. Rev. Lett. **93**, 226602 (2004); A. A. Burkov, A. S. Nunez, and A. H. MacDonald, Phys. Rev. B **70**, 155308 (2004).

[14]Roland Winkler, *Spin-Orbit Coupling Effects in Two-Dimensional Electron and Hole Systems* (Springer, Berlin, 2003).

[15]G. E. Pikus and A. N. Titkov, in *Optical Orientation*, edited by F. Meier and B. P. Zakharchenya (North-Holland, Amsterdam, 1984).

[16]E. I. Rashba, Phys. Rev. B **68**, 241315 (2003).

[17]B. L. Altshuler and A. G. Aronov, in *Electron-Electron Interactions in Disordered Systems*, edited by A. L. Efros and M. Pollak (North-Holland, Amsterdam, 1985).

[18]A. G. Malshukov and K. A. Chao, Phys. Rev. B **61**, 2413 (2000).

[19]C. Gorini, P. Schwab, R. Raimondi, and A. L. Shelankov, Phys. Rev. B **82**, 195316 (2010).

[20]A. G. Malshukov and K. A. Chao, Phys. Rev. B **71**, 121308 (2005).

[21]R. Eppenga and M. F. H. Schuurmans, Phys. Rev. B **37**, 10923 (1988).

[22]A. G. Malshukov, L. Y. Wang, C. S. Chu, and K. A. Chao, Phys. Rev. Lett. **95**, 146601 (2005).

Solid State Communications ▮ (▮▮▮▮) ▮▮▮–▮▮▮

Contents lists available at SciVerse ScienceDirect

Solid State Communications

journal homepage: www.elsevier.com/locate/ssc

Robust level coincidences in the subband structure of quasi-2D systems

R. Winkler [a,b,c,*], L.Y. Wang [c], Y.H. Lin [c], C.S. Chu [c,d]

[a] Department of Physics, Northern Illinois University, DeKalb, IL 60115, USA
[b] Materials Science Division, Argonne National Laboratory, Argonne, IL 60439, USA
[c] Department of Electrophysics, National Chiao Tung University, Hsinchu 30010, Taiwan
[d] National Center for Theoretical Sciences, Physics Division, Hsinchu 30043, Taiwan

ARTICLE INFO

Article history:
Received 14 August 2012
Accepted 5 September 2012
by F. Peeters

Keywords:
A. Semiconductors
A. Topological insulators

ABSTRACT

Recently, level crossings in the energy bands of crystals have been identified as a key signature for topological phase transitions. Using realistic models we show that the parameter space controlling the occurrence of level coincidences in energy bands has a much richer structure than anticipated previously. In particular, we identify robust level coincidences that cannot be removed by a small perturbation of the Hamiltonian compatible with the crystal symmetry. Different topological phases that are insulating in the bulk are then separated by a gapless (metallic) phase. We consider HgTe/CdTe quantum wells as a specific example.

Recently level crossings in the energy bands of crystals have become a subject of significant interest as they represent a key signature for topological phase transitions induced, e.g., by tuning the composition of an alloy or the thickness of a quasi-two-dimensional (2D) system [1–4]. For example, it was proposed [5] and soon after confirmed experimentally [6,7] that HgTe/CdTe quantum wells (QWs) show a phase transition from spin Hall insulator to a quantum spin Hall regime when the lowest electron-like and the highest hole-like subbands cross at a critical QW width of $\sim$65 Å; see also [2,8–11]. Here we present a systematic study of level crossings and anticrossings in the subband structure of quasi-2D systems. We show that the parameter space characterizing level crossings has a much richer structure than previously anticipated. In particular, we present examples for robust level coincidences that are preserved while the system parameters are varied within a finite range. Similar to the topological phase transitions characterizing the quantum Hall effect [12], the insulating Z_2 topological phases [1] thus get separated by a gapless (metallic) phase. Such an additional phase was previously predicted in Ref. [13]. Yet it was found that this phase could occur only in 3D, but not in 2D. Also, it was not clear which systems would realize such a phase. Here we take HgTe/CdTe QWs as a realistic example, though many results are relevant also for other quasi-2D systems

Level crossings were studied already in the early days of quantum mechanics [14–16]. They occur, e.g., when atoms are placed in magnetic fields in the transition region between the weak-field Zeeman effect and the high-field Paschen–Back effect. Also, they occur when molecules and solids are formed from isolated atoms. Hund [14] pointed out that adiabatic changes of 1D systems – unlike multi-dimensional systems – cannot give rise to level crossings. Von Neumann and Wigner [15] quantified how many parameters need to be varied for a level crossing. While levels of different symmetries (i.e., levels transforming according to different irreducible representations, IRs) may cross when a single parameter is varied, to achieve a level crossing among two levels of the same symmetry, it is in general necessary to vary three (two) independent parameters if the underlying eigenvalue problem is Hermitian (orthogonal). Subsequently, this problem was revisited by Herring [16] who found that the analysis by von Neumann and Wigner was not easily transferable to energy bands in a crystal due to the symmetry of the crystal potential. Similar to energy levels in finite systems, levels may coincide in periodic crystals if the levels have different symmetries. Of course, unless the crystal is invariant under inversion, this can occur only for high-symmetry lines or planes in the Brillouin zone (BZ), where the group of the wave vector is different from the trivial group C_1. If at one end point $\mathbf{k}_1$ of a line of symmetry a band with symmetry Γ_i is higher in energy than the band with symmetry Γ_j, while at the other end point $\mathbf{k}_2$ the order of Γ_i and Γ_j is reversed, these levels cross somewhere in between $\mathbf{k}_1$ and $\mathbf{k}_2$. Herring classified a level crossing as "vanishingly improbable" if it disappeared upon an infinitesimal perturbation of the crystal potential compatible with all crystal symmetries. In that sense, a level coincidence at a high-symmetry point of the BZ such as the Γ point $k=0$ becomes vanishingly improbable. For energy levels with the same symmetry, Herring derived several theorems characterizing the conditions under which level crossings may occur. In particular, he found that in

* Corresponding author at: Department of Physics, Northern Illinois University, DeKalb, IL 60115, USA.
E-mail address: rwinkler@niu.edu (R. Winkler).

0038-1098/$ - see front matter © 2012 Elsevier Ltd. All rights reserved.
http://dx.doi.org/10.1016/j.ssc.2012.09.002

the absence of inversion symmetry level crossings that are *not* vanishingly improbable may occur for isolated points $\mathbf{k}$ such that these crossings cannot be destroyed by an infinitesimal change in the crystal potential, but they occur at some point near $\mathbf{k}$. Here we identify several examples for such robust level coincidences. This illustrates that level coincidences in energy bands can be qualitatively different from level coincidences in other systems [15].

Recently, several studies focusing on topological phase transitions recognized the importance of symmetry for level crossings in energy bands [2,8–10]. Murakami et al. [2] studied the phase transition separating spin Hall insulators from the quantum spin Hall regime, focusing on generic low-symmetry configurations with and without inversion symmetry. They found that without inversion symmetry the phase transition is accompanied by a gap closing at points $\mathbf{k}$ that are not high-symmetry points. In inversion symmetric systems the gap closes only at points $\mathbf{k}=\mathbf{G}/2$ where $\mathbf{G}$ is a reciprocal lattice vector. Here we show that level crossings in quasi-2D systems can be characterized by a multitude of scenarios, taking HgTe/CdTe quantum wells as a specific example for which it is known that the lowest electron-like and the highest hole-like subbands (anti)cross for a critical QW width of about 65 Å [5–7,17]. In most semiconductors with a zinc blende structure (point group T_d) the s-antibonding orbitals form the conduction band (IR Γ_6 of T_d), whereas the p-bonding orbitals form the valence band (Γ_8 and Γ_7 of T_d). The curvature of the Γ_6 band is thus positive whereas it is negative for the Γ_8 band. For finite $\mathbf{k}$, the four-fold degenerate Γ_8 states (effective spin $j=3/2$) split into the so-called heavy hole (HH, $m_z=\pm 3/2$) and light hole (LH, $m_z=\pm 1/2$) branches. In HgTe, the order of the Γ_8 and Γ_6 bands is reversed: Γ_6 is located below Γ_8 and it has a negative (hole-like) curvature, whereas Γ_8 splits into an electron ($m_z=\pm 1/2$) and a hole ($m_z=\pm 3/2$) branch [18]. HgTe and CdTe can be combined to form a ternary alloy $Hg_xCd_{1-x}Te$, where the fundamental gap E_0 between the Γ_6 and Γ_8 bands can be tuned continuously from $E_0=+1.6$ eV in CdTe to $E_0=-0.3$ eV in HgTe with a gapless material for $x\approx 0.84$ [18]. Tuning the material composition x thus allows one to overcome Herring's conclusion [16] that a degeneracy at $k=0$ between two levels of different symmetries is, in general, vanishingly improbable.

Layers of HgTe and CdTe can also be grown epitaxially on top of each other to form QWs. At the interface the corresponding states need to be matched appropriately. The opposite signs of the effective mass inside and outside the well result in eigenstates localized at the interfaces [19]. We calculate these eigenstates as well as the corresponding subband dispersion $E_\alpha(\mathbf{k})$ using a realistic 8×8 multiband Hamiltonian $\mathcal{H}$ for the bulk bands Γ_6, Γ_8, and Γ_7, which fully takes into account important details of $E_\alpha(\mathbf{k})$ such as anisotropy, nonparabolicity, HH–LH coupling, and spin–orbit coupling both due to bulk inversion asymmetry (BIA) of the zinc blende structure of HgTe and CdTe as well as structure inversion asymmetry (SIA) of the confining potential $V(z)$. For details concerning $\mathcal{H}$ and its numerical solution see Refs. [20,21]. In the following $\mathbf{k}=(k_x,k_y)$ denotes the 2D wave vector.

The symmetry group $\mathcal{G}$ of a QW and thus the allowed level crossings depend on the crystallographic orientation of the surface used to grow a QW [a (001) surface being the most common in experiments]. It also depends on whether we have a system without or with BIA and/or SIA. The resulting point groups are summarized in Table 1. We show below that these different groups give rise to a rich parameter space for the occurrence of level coincidences. For a proper symmetry classification we project the eigenstates of $\mathcal{H}$ onto the IRs of the respective point group [22]. In the following, all IRs are labeled according to Koster et al. [23]. As spin–orbit coupling plays a crucial role for BIA and SIA [20] as well as for topological phase transitions [1–4], all IRs referred to in this work are double-group IRs. For comparison,

Table 1
The point group of a QW for different growth directions starting from a bulk semiconductor with diamond structure (point group O_h) or zinc blende structure (point group T_d) for a system without ("sym.") or with ("asym.") SIA.

Bulk		[001]	[111]	[110]	[mmn]	[0mn]	[lmn]	Axial appr.
O_h	sym.	D_{4h}	D_{3d}	D_{2h}	C_{2h}	C_{2h}	C_i	$D_{\infty h}$
	asym.	C_{4v}	C_{3v}	C_{2v}	C_s	C_s	C_1	$C_{\infty v}$
T_d	sym.	D_{2d}	C_{3v}	C_{2v}	C_s	C_2	C_1	$D_{\infty h}$
	asym.	C_{2v}	C_{3v}	C_s	C_s	C_1	C_1	$C_{\infty v}$

Table 1 also lists the point groups if the prevalent axial (or spherical) approximation is used for $\mathcal{H}$. In this approximation, BIA is ignored and different surface orientations become indistinguishable.

First we neglect the small terms in $\mathcal{H}$ due to BIA so that the bulk Hamiltonian has the point group O_h. In the absence of SIA, a quasi-2D system grown on a (001) surface has the point group D_{4h} (which includes inversion) and all electron and hole states throughout the BZ are two-fold degenerate [22]. Subband edges $k=0$ in a HgTe/CdTe QW as a function of well width w are shown in Fig. 1(a). The HH states transform according to $\Gamma_6^\pm$ of D_{4h}. The electron-like and LH-like subbands transform according to $\Gamma_7^\pm$. As expected, the $\Gamma_6^\pm$ and $\Gamma_7^\pm$ subbands may cross as a function of w.

In the presence of SIA we cannot classify the eigenstates anymore according to their behavior under parity. Without BIA the point group becomes C_{4v}. HH states transform according to Γ_6 of C_{4v} and electron- and LH-like states transform according to Γ_7. The level crossings depicted in Fig. 1(a) remain allowed in this case [8,24].

The situation changes when taking into account BIA. Without SIA the point group becomes D_{2d}. In this case, all subbands transform alternately according to the IRs Γ_6 and Γ_7 of D_{2d}, irrespective of the dominant spinor components. In particular, both the highest HH state and the lowest conduction band state transform according to Γ_6 of D_{2d} so that around $w\simeq 65$ Å we obtain an anticrossing between these levels of about 2.9 meV (for $k=0$), see Fig. 1(b) [8–10]. With both BIA and SIA the point group becomes C_{2v}. Now we have only one double-group IR Γ_5. Thus it follows readily that all subbands anticross as a function of a continuous parameter such as the well width.

While BIA opens a gap at $k=0$, level coincidences remain possible for some $\tilde{\mathbf{k}}\neq 0$ when the well width w is tuned to a critical value $\tilde{w}$ [2,16]. Considering a (001) surface with BIA, we find, indeed, that for each direction ϕ of $\mathbf{k}=(k,\phi)$, critical values $\tilde{w}$ and $\tilde{k}$ exist that give rise to a band crossing. Thus we get a line in $\mathbf{k}$ space where the bands cross when w is varied within some finite range. This result holds for QWs on a (001) surface with BIA, without and with SIA (as studied experimentally in Refs. [6,7]). As an example, Fig. 2(a) shows $\tilde{\mathbf{k}}$ in the presence of a perpendicular electric field $\mathcal{E}_z=100$ kV/cm.

In general, three independent parameters must be tuned for a level coincidence in a quantum mechanical systems [15] if the underlying eigenvalue problem is Hermitian. While the multiband Hamiltonian $\mathcal{H}$ used here [20] is likewise Hermitian (not orthogonal), only two independent parameters (w and $k=|\mathbf{k}|$) are necessary to achieve the level degeneracy. We have here an example for the robustness of band coincidences under perturbations that was predicted by Herring [16] to occur in systems without a center of inversion (in multiples of four). It shows that level coincidences in energy bands can behave qualitatively different from level coincidences in other quantum mechanical systems [15]. We note that the band coincidences found here are not protected by symmetry in the sense that – unlike the other

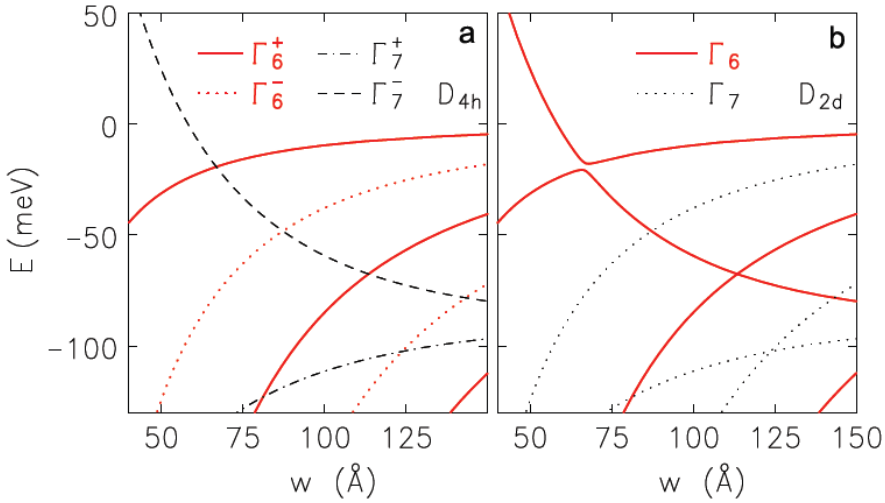

Fig. 1. (Color online) Subband states in a symmetric HgTe/CdTe quantum well (for $k=0$) as a function of well width w calculated with an 8×8 Hamiltonian (a) neglecting BIA (point group D_{4h}) and (b) with BIA (D_{2d}). States transforming according to $\Gamma_6^{\pm}$ of D_{4h} (Γ_6 of D_{2d}) are shown in red; states shown in black transform according to $\Gamma_7^{\pm}$ of D_{4h} (Γ_7 of D_{2d}).

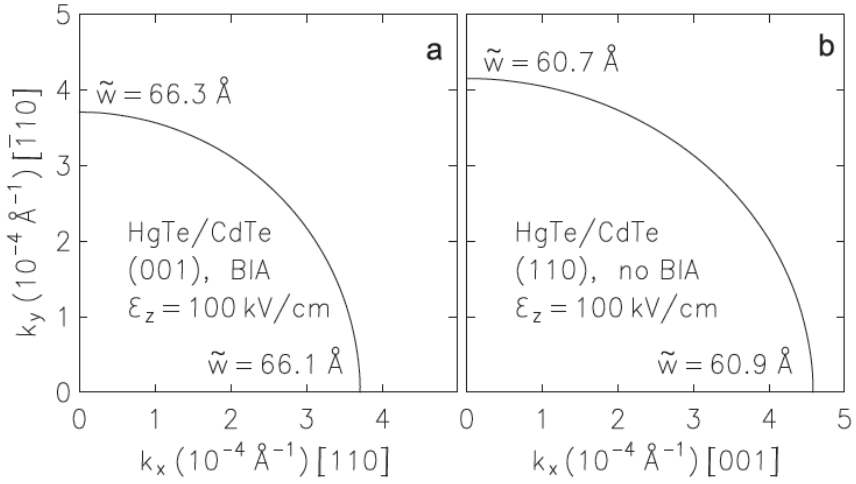

Fig. 2. Critical wave vectors $\tilde{\mathbf{k}}$ that give rise to a level coincidence in a HgTe/CdTe QW (a) on a (001) surface taking into account BIA (b) on a (110) surface neglecting BIA. In both cases a perpendicular field $\mathcal{E}_z=100$ kV/cm was assumed. In (a) the level coincidence requires a well width $\tilde{w}=66.1$ Å for $\tilde{\mathbf{k}}\|[110]$ and $\tilde{w}=66.3$ Å for $\tilde{\mathbf{k}}\|[\bar{1}10]$. In (b) we have $\tilde{w}=60.9$ Å for $\tilde{\mathbf{k}}\|[001]$ and $\tilde{w}=60.7$ Å for $\tilde{\mathbf{k}}\|[\bar{1}10]$.

cases discussed above – the group of $\tilde{\mathbf{k}}$ is the trivial group C_1 containing only the identity.

The situation is different for quasi-2D systems grown on a (111) surface. In the absence of BIA and SIA, the point group is D_{3d}. HH states at $k=0$ transform according to the complex conjugate IRs $\Gamma_5^+\oplus\Gamma_6^+$ or $\Gamma_5^-\oplus\Gamma_6^-$, where $\oplus$ indicates that these IRs must be combined due to time reversal symmetry. All other subband edges transform according to $\Gamma_4^{\pm}$. In the presence of BIA and/or SIA the point group becomes C_{3v}. Then HH states transform according to the complex conjugate IRs $\Gamma_5\oplus\Gamma_6$. Electron-like and LH-like states transform according to Γ_4. Thus it follows that on a (111) surface the HH states always cross the other states at $k=0$ as a function of w [similar to Fig. 1(a)]. The IRs for different geometries starting out from a (001) or (111) surface are summarized in Table 2.

Finally we consider quasi-2D states on a (110) surface. In the absence of BIA and SIA, the point group becomes D_{2h}. Here, all subbands transform alternately according to Γ_5^+ and Γ_5^- with the topmost HH-like subband being Γ_5^+ and the lowest electron-like subband being Γ_5^-. A level crossing as a function of w is thus again allowed at $k=0$. In the presence of either BIA or SIA the symmetry is reduced to C_{2v}. While the point group in both cases is the same [25], we obtain a remarkable difference between these cases. With SIA the level crossing occurs for a line in $\mathbf{k}$ space, similar to the (001) surface, see Fig. 2(b). With BIA we obtain a level

Table 2
Irreducible representations of quasi-2D states ($\mathbf{k}=0$) on a (001) and (111) surface, starting from a bulk semiconductor with diamond (point group O_h) or zinc blende (point group T_d) structure for a system without ("sym.") or with ("asym.") structure inversion asymmetry.

Bulk		(001)			(111)		
		Group	c, LH	HH	Group	c, LH	HH
O_h	sym.	D_{4h}	$\Gamma_7^{\pm}$	$\Gamma_6^{\pm}$	D_{3d}	$\Gamma_4^{\pm}$	$\Gamma_5^{\pm}\oplus\Gamma_6^{\pm}$
	asym.	C_{4v}	Γ_7	Γ_6	C_{3v}	Γ_4	$\Gamma_5\oplus\Gamma_6$
T_d	sym.	D_{2d}	$\Gamma_{7/6}$	$\Gamma_{6/7}$	C_{3v}	Γ_4	$\Gamma_5\oplus\Gamma_6$
	asym.	C_{2v}	Γ_5	Γ_5	C_{3v}	Γ_4	$\Gamma_5\oplus\Gamma_6$

crossing only for $\mathbf{k}\|[\bar{1}10]$ with $\tilde{k} \approx 0.0012$ Å^{-1} and $\tilde{w} \approx 62.5$ Å, thus giving an example for the level crossings occurring for isolated points $\tilde{\mathbf{k}} \neq 0$ as discussed by Murakami et al. [2]. These examples illustrate that the occurrence of level crossings at either isolated points or along continuous lines in parameter space is not simply related with the system symmetry [25]. In the presence of both BIA and SIA (group C_s) we have the same situation as with BIA only, i.e., adding SIA changes the values of $\tilde{k}$ and $\tilde{w}$, but we keep $\tilde{\mathbf{k}}\|[\bar{1}10]$.

In conclusion, we have shown that a rich parameter space characterizes the occurrence of level coincidences in the subband structure of quasi-2D systems. In particular, we have identified level coincidences for wave vectors $\tilde{\mathbf{k}} \neq 0$ that cannot be removed by a small perturbation of the Hamiltonian compatible with the QW symmetry [16]. Taking into account the full crystal symmetry of real materials is an important difference between the current analysis and previous work that considered only lattice periodicity, inversion and time reversal symmetry. The full set of symmetries imposes additional constraints on the band Hamiltonian beyond the torus topology of the BZ that reflects the translational symmetry. These additional constraints generally reduce the number of parameters that are required to obtain level crossings [16] so that robust level coincidences can be achieved even in quasi-2D systems. As quasi-2D systems can be designed and manipulated in various ways not available in 3D this opens new avenues for both experimental and theoretical research of topologically nontrivial materials.

As a specific example, we have considered HgTe/CdTe QWs, where a particular level crossing reflects a topological phase transition from spin Hall insulator to a quantum spin Hall regime [5–7]. The robustness of the level coincidences found here implies that these phases, which are insulating in the bulk, are separated by a gapless phase similar to the metallic phases that separate the insulating quantum Hall phases [12]. While in HgTe/CdTe QWs the range of critical well widths $\tilde{w}$ giving rise to the metallic phase is rather small (about 0.1 monolayers), we expect that future research will be able to identify materials showing larger parameter ranges that can be probed more easily in experiments. We note that our symmetry-based classification of level crossings is independent of specific numerical values of the band structure parameters entering the Hamiltonian $\mathcal{H}$. Indeed, our findings are directly applicable also to other quasi-2D systems made of bulk semiconductors with a zinc blende or diamond structure such as hole subbands in GaAs/AlGaAs and SiGe quantum wells. In general, the $\mathbf{k}\cdot\mathbf{p}$ coupling between the LH1 (Γ_7^+ of D_{4h}) and HH2 (Γ_6^-) subbands gives rise to an electron-like dispersion of the LH1 subband for small wave vectors k [26]. If these subbands become (nearly) degenerate at $k=0$, the coupling between these subbands becomes the dominant effect. This situation is described by the same effective Hamiltonian that characterizes the subspace consisting of the lowest electron and highest HH subband in a HgTe/CdTe QW [5]. It can be exploited if biaxial strain is used to tune the separation between the LH1 and HH2 subbands [27].

Acknowledgments

R.W. appreciates stimulating discussions with T. Hirahara, A. Hoffmann, L.W. Molenkamp, and S. Murakami. He thanks the Kavli Institute for Theoretical Physics China at the Chinese Academy of Sciences for hospitality and support during the early stage of this work. This work was supported by Taiwan NSC (Contract nos. 99-2112-M-009-006 and 100-2112-M-009-019) and a MOE-ATU Grant. Work at Argonne was supported by DOE BES under Contract no. DE-AC02-06CH11357.

References

[1] C.L. Kane, E.J. Mele, Phys. Rev. Lett. 95 (2005) 146802;
C.L. Kane, E.J. Mele, Phys. Rev. Lett. 95 (2005) 226801.
[2] S. Murakami, S. Iso, Y. Avishai, M. Onoda, N. Nagaosa, Phys. Rev. B 76 (2007) 205304.
[3] M.Z. Hasan, C.L. Kane, Rev. Mod. Phys. 82 (2010) 3045.
[4] X.-L. Qi, S.-C. Zhang arXiv:1008.2026.
[5] B.A. Bernevig, T.L. Hughes, S.-C. Zhang, Science 314 (2006) 1757.
[6] M. König, S. Wiedmann, C. Brüne, A. Roth, H. Buhmann, L.W. Molenkamp, X.-L. Qi, S.-C. Zhang, Science 318 (2007) 766.
[7] A. Roth, C. Brüne, H. Buhmann, L.W. Molenkamp, J. Maciejko, X.-L. Qi, S.-C. Zhang, Science 325 (2009) 294.
[8] M. König, H. Buhmann, L.W. Molenkamp, T. Hughes, C.-X. Liu, X.-L. Qi, S.-C. Zhang, J. Phys. Soc. Jpn. 77 (2008) 031007.
[9] C. Liu, T.L. Hughes, X.-L. Qi, K. Wang, S.-C. Zhang, Phys. Rev. Lett. 100 (2008) 236601.
[10] X. Dai, T.L. Hughes, X.-L. Qi, Z. Fang, S.-C. Zhang, Phys. Rev. B 77 (2008) 125319.
[11] J.-W. Luo, A. Zunger, Phys. Rev. Lett. 105 (2010) 176805.
[12] D.J. Thouless, M. Kohmoto, M.P. Nightingale, M. den Nijs, Phys. Rev. Lett. 49 (1982) 405.
[13] S. Murakami, New J. Phys. 9 (2007) 356.
[14] F. Hund, Z. Phys. 40 (1927) 742.
[15] J. von Neumann, E. Wigner, Phys. Z. 30 (1929) 467.
[16] C. Herring, On energy coincidences in the theory of Brillouin zones, Ph.D. Thesis, Princeton University, Princeton, NJ, 1937; C. Herring, Phys. Rev. 52 (1937) 365.
[17] A. Pfeuffer-Jeschke, Bandstruktur und Landau-Niveaus quecksilberhaltiger II-VI-Heterostrukturen, Ph.D. Thesis, University of Würzburg, Würzburg, Germany, 2000.
[18] R. Dornhaus, G. Nimtz, B. Schlicht, Narrow-Gap Semiconductors, Springer, Berlin, 1983.
[19] Y.R. Lin-Liu, L.J. Sham, Phys. Rev. B 32 (1985) 5561.
[20] R. Winkler, Spin–Orbit Coupling Effects in Two-Dimensional Electron and Hole Systems, Springer, Berlin, 2003.
[21] In our calculations for HgTe/CdTe QWs, we use the band parameters of E.G. Novik, et al., Phys. Rev. B 72 (2005) 035321. In the Γ_8 and Γ_7 bands, BIA results in k linear terms proportional to C_k, see M. Cardona, et al., Phys. Rev. Lett. 56 (1986) 2831. In the off-diagonal blocks of $\mathcal{H}$ coupling the Γ_6 with the Γ_8 and Γ_7 bands we also have terms quadratic in k weighted by $B_{8v}^{\pm}$ and B_{7v} [20]. We estimate $B_{8v}^{+} \simeq B_{7v} = -20$ eV Å^2 and $B_{8v}^{-} = 1$ eV Å^2.
[22] G.L. Bir, G.E. Pikus, Symmetry and Strain-Induced Effects in Semiconductors, Wiley, New York, 1974.
[23] G.F. Koster, J.O. Dimmock, R.G. Wheeler, H. Statz, Properties of the Thirty-Two Point Groups, MIT, Cambridge, MA, 1963.
[24] D.G. Rothe, R.W. Reinthaler, C.-X. Liu, L.W. Molenkamp, S.-C. Zhang, E.M. Hankiewicz, New J. Phys. 12 (2010) 065012.
[25] 2D systems on a (110) surface with either BIA or SIA have the point group C_{2v}. Yet with SIA the symmetry axis of C_{2v} is perpendicular to the (110) plane, whereas with BIA this axis is along the in-plane [001] axis.
[26] D.A. Broido, L.J. Sham, Phys. Rev. B 31 (1985) 888.
[27] P. Voisin, C. Delalande, M. Voos, L.L. Chang, A. Segmuller, C.A. Chang, L. Esaki, Phys. Rev. B 30 (1984) 2276.

Works in preparation:

"Effects of spin-orbit interaction on the topological physics in a 2D triangular muffin-potential lattice"

R.S. Chang, W.L. Su, and C.S. Chu

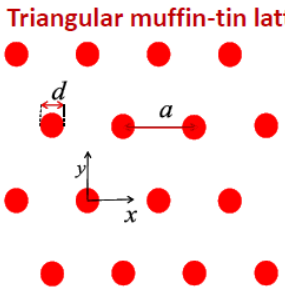

$$H = \frac{p^2}{2m^*} + V + H_{\mathrm{soI}},$$

$$V = \sum_n V_{\mathrm{MT}}(\vec{r} - \vec{R}_n),$$

$$V_{\mathrm{MT}}(r > d/2) = 0; \qquad V_{\mathrm{MT}}(r < d/2) = U_0,$$

$$H_{\mathrm{SOI}} = -\frac{\lambda}{\hbar}\vec{\sigma}\cdot\left(\vec{\nabla}V \times \vec{p}\right); \qquad \lambda = 120\text{Å}^2 \text{ (for InAs)}$$

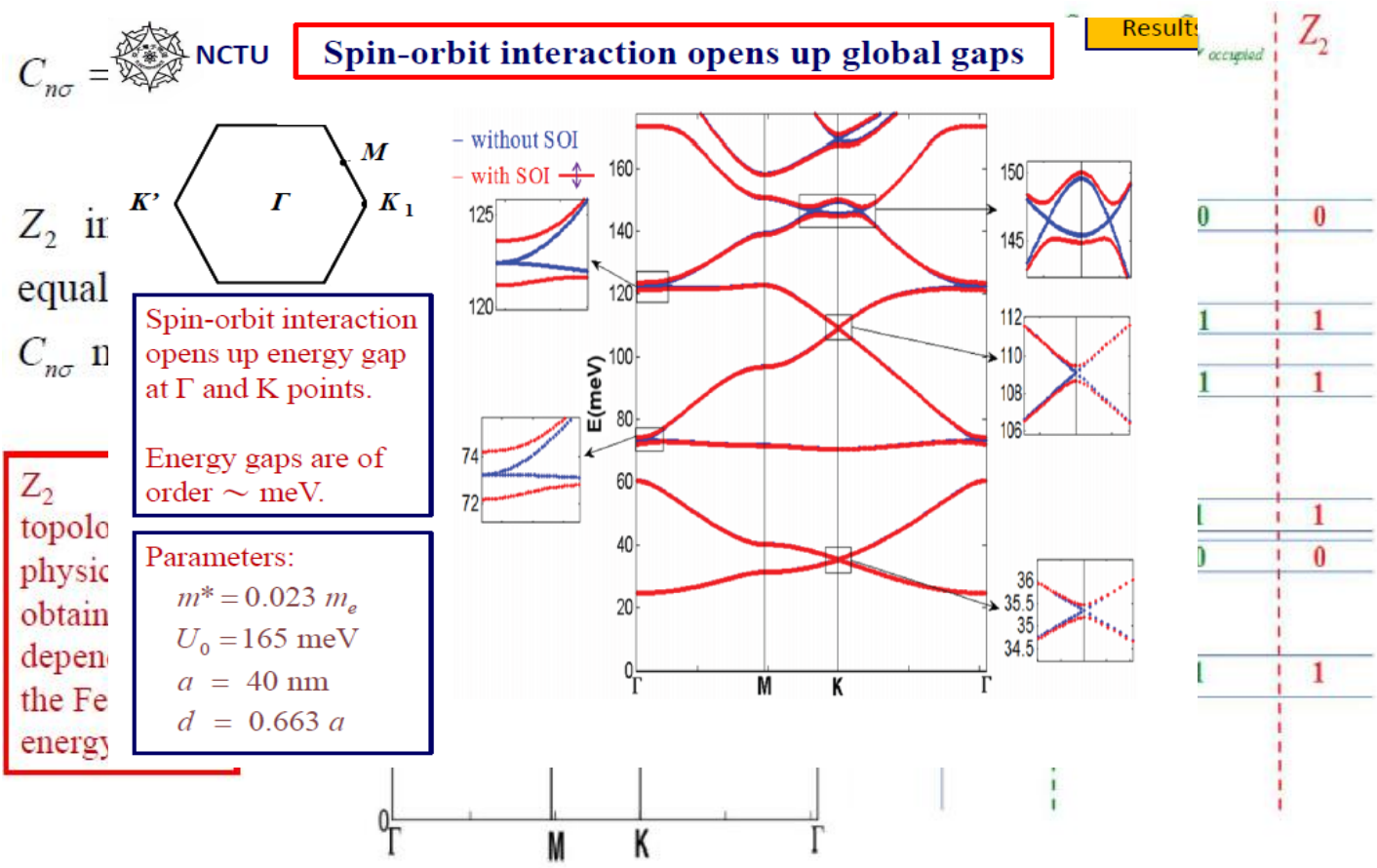

$$C_{n\sigma} = \frac{(C_{n\uparrow} - C_{n\downarrow})}{2}$$

Z_2 invariant equals $C_{n\sigma}$ mode 2

Z_2 topological physics is obtained, depending on the Fermi energy.

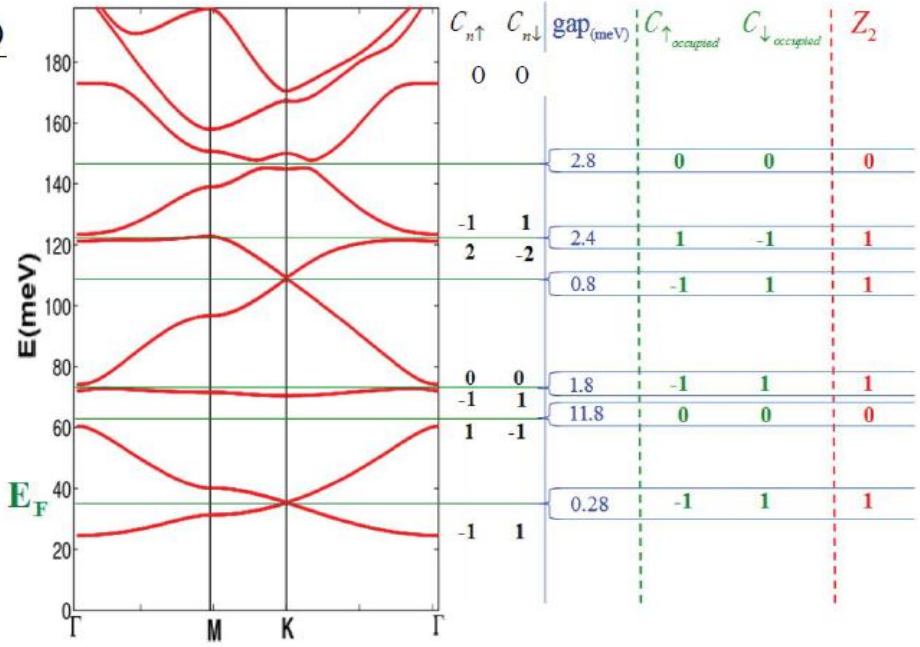

Energy gap dependences on the aspect ratio of the muffin-tin lattice potential

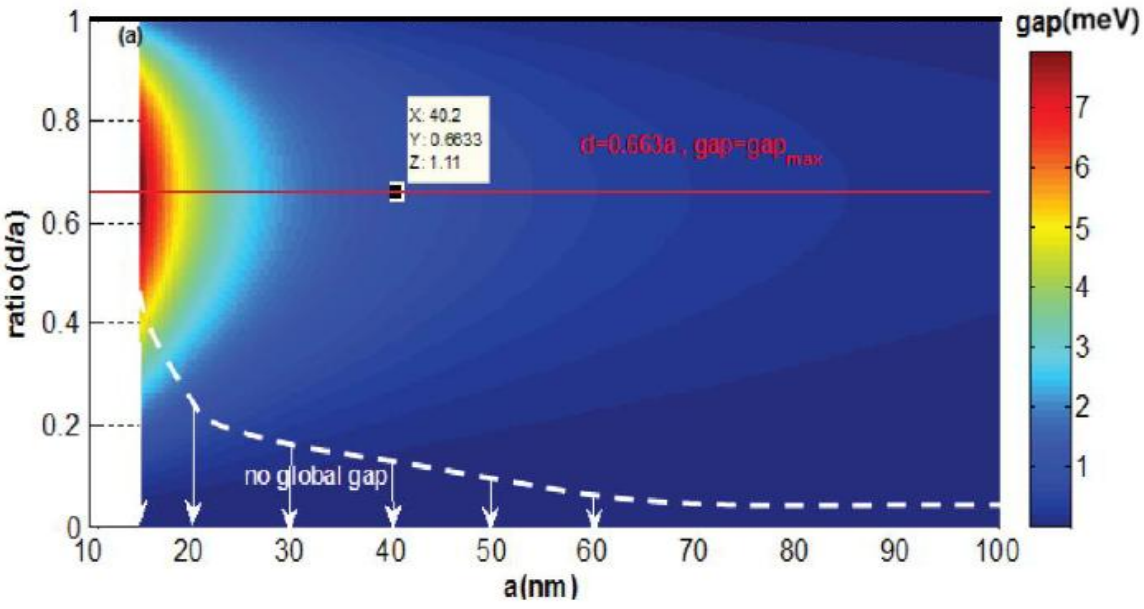

國科會補助專題研究計畫成果報告自評表

請就研究內容與原計畫相符程度、達成預期目標情況、研究成果之學術或應用價值（簡要敘述成果所代表之意義、價值、影響或進一步發展之可能性）、是否適合在學術期刊發表或申請專利、主要發現或其他有關價值等，作一綜合評估。

1. 請就研究內容與原計畫相符程度、達成預期目標情況作一綜合評估 ■→達成目標 □ 未達成目標（請說明，以 100 字為限） □ 實驗失敗 □ 因故實驗中斷 □ 其他原因 說明：
2. 研究成果在學術期刊發表或申請專利等情形： 論文：■已發表 □未發表之文稿 ■撰寫中 □無 專利：□已獲得 □申請中 □無 技轉：□已技轉 □洽談中 □無 其他：（以 100 字為限）

3. 請依學術成就、技術創新、社會影響等方面，評估研究成果之學術或應用價值（簡要敘述成果所代表之意義、價值、影響或進一步發展之可能性）（以 500 字為限）

The findings that we have obtained in this project are many. Two major parts are:

1. Impact on the topological physics research:

   A. *Edge-states generation at an armchair-graphene open boundary*:

   In this finding, not only that we have shown that edge-states can be generated at an armchair-graphene open boundary by an edge-potential, we have also shown that the edge-states are non-Tamm-like. This peculiar nature of the edge-state, namely, that there is no threshold edge-potential for the edge-state generation, is very interesting, and is worth further exploration. It is because one might wonder whether there is topological origin in this edge-state formation, and if it did, how to identify it.

   Equally importantly, we have shown that the physical mechanism that makes possible the edge-state formation is the turning on of pseudospin-flipping scattering at the open boundary. This is confirmed by our finding of out-of-plane pseudospin spatial distribution when a valley-polarized beam incident upon an open boundary. We have also studied the contribution to these edge-states to the conductance in an armchair-graphene nanoribbon. The chirality of the edge-states is expected to cause their conductance to be more robust against disorder. This, again, is worth further exploration.

   B. *Effects of structure-inversion asymmetry (SIA) and bulk-inversion asymmetry (BIA) on the topological physics in HgTe quantum well structures*:

   With the introduction of the BIA to the 8×8 Luttinger Hamiltonian, we have shown that the $\vec{k}_{\|}=0$ energy levels in the HgTe quantum well exhibits level anti-crossing at a well width very close to the well known critical well width for level-crosing, had the BIA were not introduced. The question whether this would destroy the topological physics is answered in this work. We show that the 2D Hamiltonian of the HgTe quantum well still contains gapless (or level-crossing) features. We further calculate explicitly the edge states, their wavefunction, and their contribution to the conductance in a quantum channel that is formed out of the quantum well. The conductance characteristics for a quantum channel with a potential region, and with or without BIA terms, are studied in light of the Fano processes. Our results show that the BIA term has not destroyed the topological nature of the system, but has distinct effects on the transmission characteristics. This study gives insight upon the robustness of the topological features in well known topological systems.

   C. *Topological physics in a 2D muffin-tin potential triangular lattice*:

   In this work, we find out that by introducing a spin-orbit interaction that comes together with the muffin-tin potential lattice on a 2D semiconductor substrate, the system exhibits Z_2 physics. The Chern numbers of individual energy bands are calculated and the optimal lattice configurations for the energy gap are obtained. This work provides insight for the possibility of driving a normal system into a topologically non-trivial regime.

2. Nonuniversality of the intrinsic inverse spin-Hall effect in diffusive systems:

   We find out that the factor relating the electric and spin currents is not universal, and depends on the origin of the spin current.

國科會補助專題研究計畫項下出席國際學術會議心得報告

日期：___年___月___日

計畫編號	NSC-100－2112－M－009－019－		
計畫名稱	奈米圖樣化的二維電子系統中拓樸絕緣體物理之研究		
出國人員姓名	朱仲夏	服務機構及職稱	國立交通大學電子物理系
會議時間	2012年2月27 至 2012年3月2日	會議地點	Boston, USA
會議名稱	(中文)美國物理學會物理年會 2012年三月會議 (英文) American Physical Society (APS) March Meeting 2012		
發表論文題目	(英文)Effects of spin-orbit interaction on a triangular lattice potential patterned two-dimensional electron gas		

一、參加會議經過:

The APS march meeting was from Feb. 27 (Monday) to March 2 (Friday). My group had three talks to present in this meeting: on Monday, Thursday, and Friday, all on the morning. So we arrived Boston on Feb. 26 (Sunday) afternoon, and leave on March 3 (Saturday) morning.

The first talk, by my postdoctoral research associate Dr. L.Y. Wang, was in the Session A32: Topological Insulators: Quantum Hall Effects. The title of the talk was: "Topological property for magnetic flux tubes in a two-dimensional electron gas".

The second talk, by my Ph.D. student Mr. C.H. Chiu, was in the Session V11: Focus Session: Graphene Structure, Stacking, Interactions; edges and grain boundaries". The title of the talk was: "Effects of edge-potential on an armchair-graphene open boundary and nanoribbon".

The third talk, my myself, was in the Session Y32: Topological Insulators: General theory. The title of the talk was: "Effects of spin-orbit interaction on a triangular lattice potential patterned two-dimensional electron gas".

The second and the third talks have each drawn a number of responses and discussions after the presentation. We considered them well received.

In between our talks, we have attended sessions mostly focusing on topological physics and graphene related topics. There were many sessions on these two general topics.

二、與會心得

I think that we had done a good job in presenting the work of my group. Given the limited time for each presentation, we managed to post questions in the beginning of our talk to best motivate the need of our work. And we presented, in the outset, a summary of our work, which will appear again at the end of the talk. This helped registering in the audience the take-home main messages of our work. The main message in every powerpoint page has to be stated explicitly. A lot of work and time has been done to organize our powerpoint, and to make the presentation of equations as friendly as possible. I think going through this painstaking process and the experience of presenting to an audience of close to hundred physicists has had important impact to my postdoc and my Ph.D. student. And allowing younger generation to present their work in such an international event is worth the cost of supporting their trip.

三、考察參觀活動(無是項活動者略)

四、建議

More generous support for serious Ph.D. students and post-docs to present their work in important international conferences.

五、攜回資料名稱及內容

六、其他

國科會補助專題研究計畫項下出席國際學術會議心得報告

日期：___年___月___日

計畫編號	NSC-100－2112－M－009－019－		
計畫名稱	奈米圖樣化的二維電子系統中拓樸絕緣體物理之研究		
出國人員姓名	朱仲夏	服務機構及職稱	國立交通大學電子物理系
會議時間	2012年2月27 至 2012年3月2日	會議地點	Boston, USA
會議名稱	(中文)美國物理學會物理年會 2012年三月會議 (英文) American Physical Society (APS) March Meeting 2012		
發表論文題目	(英文)Effects of spin-orbit interaction on a triangular lattice potential patterned two-dimensional electron gas		

一、參加會議經過:

The APS march meeting was from Feb. 27 (Monday) to March 2 (Friday). My group had three talks to present in this meeting: on Monday, Thursday, and Friday, all on the morning. So we arrived Boston on Feb. 26 (Sunday) afternoon, and leave on March 3 (Saturday) morning.

The first talk, by my postdoctoral research associate Dr. L.Y. Wang, was in the Session A32: Topological Insulators: Quantum Hall Effects. The title of the talk was: "Topological property for magnetic flux tubes in a two-dimensional electron gas".

The second talk, by my Ph.D. student Mr. C.H. Chiu, was in the Session V11: Focus Session: Graphene Structure, Stacking, Interactions; edges and grain boundaries". The title of the talk was: "Effects of edge-potential on an armchair-graphene open boundary and nanoribbon".

The third talk, my myself, was in the Session Y32: Topological Insulators: General theory. The title of the talk was: "Effects of spin-orbit interaction on a triangular lattice potential patterned two-dimensional electron gas".

The second and the third talks have each drawn a number of responses and discussions after the presentation. We considered them well received.

In between our talks, we have attended sessions mostly focusing on topological physics and graphene related topics. There were many sessions on these two general topics.

二、與會心得

I think that we had done a good job in presenting the work of my group. Given the limited time for each presentation, we managed to post questions in the beginning of our talk to best motivate the need of our work. And we presented, in the outset, a summary of our work, which will appear again at the end of the talk. This helped registering in the audience the take-home main messages of our work. The main message in every powerpoint page has to be stated explicitly. A lot of work and time has been done to organize our powerpoint, and to make the presentation of equations as friendly as possible. I think going through this painstaking process and the experience of presenting to an audience of close to hundred physicists has had important impact to my postdoc and my Ph.D. student. And allowing younger generation to present their work in such an international event is worth the cost of supporting their trip.

三、考察參觀活動(無是項活動者略)

四、建議

More generous support for serious Ph.D. students and post-docs to present their work in important international conferences.

五、攜回資料名稱及內容

六、其他

國科會補助計畫衍生研發成果推廣資料表

日期:2012/11/05

國科會補助計畫	計畫名稱: 奈米圖樣化的二維電子系統中拓樸絕緣體物理之研究
	計畫主持人: 朱仲夏
	計畫編號: 100-2112-M-009-019- 學門領域: 半導體物理－理論

無研發成果推廣資料

100 年度專題研究計畫研究成果彙整表

計畫主持人：朱仲夏	計畫編號：100-2112-M-009-019-
計畫名稱：奈米圖樣化的二維電子系統中拓樸絕緣體物理之研究	

成果項目			量化			單位	備註（質化說明：如數個計畫共同成果、成果列為該期刊之封面故事...等）
			實際已達成數（被接受或已發表）	預期總達成數(含實際已達成數)	本計畫實際貢獻百分比		
國內	論文著作	期刊論文	0	0	100%	篇	
		研究報告/技術報告	0	0	100%		
		研討會論文	0	0	100%		
		專書	0	0	100%		
	專利	申請中件數	0	0	100%	件	
		已獲得件數	0	0	100%		
	技術移轉	件數	0	0	100%	件	
		權利金	0	0	100%	千元	
	參與計畫人力（本國籍）	碩士生	0	0	100%	人次	
		博士生	0	0	100%		
		博士後研究員	0	0	100%		
		專任助理	0	0	100%		
國外	論文著作	期刊論文	3	3	100%	篇	
		研究報告/技術報告	0	0	100%		
		研討會論文	0	0	100%		
		專書	0	0	100%	章/本	
	專利	申請中件數	0	0	100%	件	
		已獲得件數	0	0	100%		
	技術移轉	件數	0	0	100%	件	
		權利金	0	0	100%	千元	
	參與計畫人力（外國籍）	碩士生	3	0	100%	人次	
		博士生	2	0	100%		
		博士後研究員	1	0	100%		
		專任助理	0	0	100%		

其他成果 (無法以量化表達之成果如辦理學術活動、獲得獎項、重要國際合作、研究成果國際影響力及其他協助產業技術發展之具體效益事項等，請以文字敘述填列。)	A paper Phy.Rev. B 85, 155444 (2012) has been included into the Virtual Journal of Nanoscale Science and Technology -May 7, 2012 (Vol. 25, Issue 19).

	成果項目	量化	名稱或內容性質簡述
科教處計畫加填項目	測驗工具(含質性與量性)	0	
	課程/模組	0	
	電腦及網路系統或工具	0	
	教材	0	
	舉辦之活動/競賽	0	
	研討會/工作坊	0	
	電子報、網站	0	
	計畫成果推廣之參與（閱聽）人數	0	

國科會補助專題研究計畫成果報告自評表

請就研究內容與原計畫相符程度、達成預期目標情況、研究成果之學術或應用價值（簡要敘述成果所代表之意義、價值、影響或進一步發展之可能性）、是否適合在學術期刊發表或申請專利、主要發現或其他有關價值等，作一綜合評估。

1. 請就研究內容與原計畫相符程度、達成預期目標情況作一綜合評估

■達成目標

□未達成目標（請說明，以 100 字為限）

□實驗失敗

□因故實驗中斷

□其他原因

說明：

2. 研究成果在學術期刊發表或申請專利等情形：

論文：■已發表 □未發表之文稿 □撰寫中 □無

專利：□已獲得 □申請中 ■無

技轉：□已技轉 □洽談中 ■無

其他：(以 100 字為限)

3. 請依學術成就、技術創新、社會影響等方面，評估研究成果之學術或應用價值（簡要敘述成果所代表之意義、價值、影響或進一步發展之可能性）(以 500 字為限)

Impact on academic research:

1. On the topological physics:

A. Edge-state generation on an armchair-graphene open boundary

B. Effects of structural-inversion asymmetry and bulk-inversion asymmetry on the topological physics in HgTe quantum well structures

C. Topological physics in a 2D muffin-tin potential triangular lattice

2. Nonuniversality of the intrinsic inverse spin-Hall effect in diffusive systems

Impact on society:

Both topological physical systems and graphene are important systems for future electronic technology and for energy saving technology.